

ไฮโดรดีออกซิเจนชั้นของกรดโอเลอิกบนตัวเร่งปฏิกิริยาซัลไฟด์ของ Co-Mo และ Ni-Mo แบบไม่
มีตัวรองรับ



นางสาวปภาวี แสงงาม

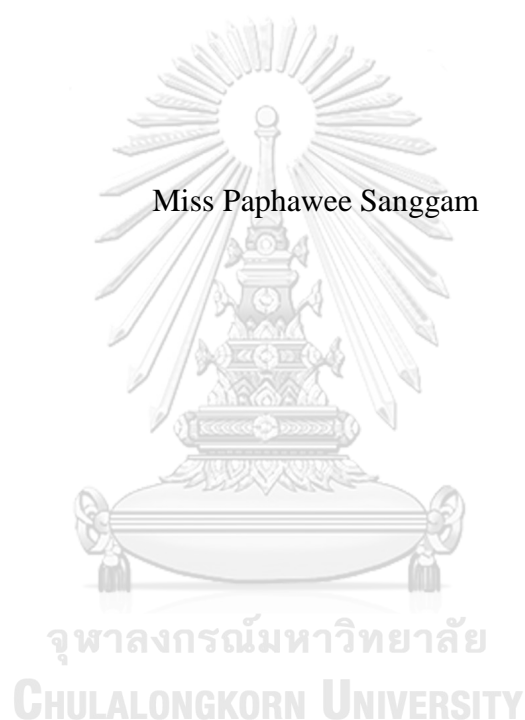
จุฬาลงกรณ์มหาวิทยาลัย

บทคัดย่อและแฟ้มข้อมูลฉบับเต็มของวิทยานิพนธ์ตั้งแต่ปีการศึกษา 2554 ที่ให้บริการในคลังปัญญาจุฬาฯ (CUIR)
เป็นแฟ้มข้อมูลของนิสิตเจ้าของวิทยานิพนธ์ ที่ส่งผ่านทางบัณฑิตวิทยาลัย

The abstract and full text of theses from the academic year 2011 in Chulalongkorn University Intellectual Repository (CUIR)
are the thesis authors' files submitted through the University Graduate School.

วิทยานิพนธ์นี้เป็นส่วนหนึ่งของการศึกษาตามหลักสูตรปริญญาวิทยาศาสตรมหาบัณฑิต
สาขาวิชาปิโตรเคมีและวิทยาศาสตร์พอลิเมอร์
คณะวิทยาศาสตร์ จุฬาลงกรณ์มหาวิทยาลัย
ปีการศึกษา 2560
ลิขสิทธิ์ของจุฬาลงกรณ์มหาวิทยาลัย

HYDRODEOXYGENATION OF OLEIC ACID ON UNSUPPORTED Co-Mo AND
Ni-Mo SULFIDE CATALYSTS



A Thesis Submitted in Partial Fulfillment of the Requirements
for the Degree of Master of Science Program in Petrochemistry and Polymer Science
Faculty of Science
Chulalongkorn University
Academic Year 2017
Copyright of Chulalongkorn University

ปกาวี แสงงาม : ไฮโดรดีออกซิเจนชั้นของกรดโอเลอิกบนตัวเร่งปฏิกิริยาซัลไฟด์ของ Co-Mo และ Ni-Mo แบบไม่มีตัวรองรับ (HYDRODEOXYGENATION OF OLEIC ACID ON UNSUPPORTED Co-Mo AND Ni-Mo SULFIDE CATALYSTS) อ. ที่ปริกษาวิทยานิพนธ์หลัก: ศ. ดร. ภัทรพรรณ ประศาสน์สารกิจ, อ. ที่ปริกษาวิทยานิพนธ์ร่วม: ดร. บุญญาวินัยอยู่สุข, 84 หน้า.

งานวิจัยนี้ศึกษาไฮโดรดีออกซิเจนชั้นของกรดโอเลอิก (สารจำลองน้ำมันปาล์ม) ด้วยตัวเร่งปฏิกิริยาซัลไฟด์ของ Co-Mo และ Ni-Mo แบบไม่มีตัวรองรับ เพื่อผลิตน้ำมันดีเซลชีวภาพสังเคราะห์ในเครื่องปฏิกรณ์ Parr โดยตัวแปรที่ศึกษาคือ อุณหภูมิ ความดัน และอัตราส่วนโดยโมลของตัวเร่งปฏิกิริยา จากการศึกษาพบว่าผลิตภัณฑ์หลักคือสารประกอบนอร์มัลอัลเคน C₁₇ และ C₁₈ โดยการเพิ่มความดันส่งผลให้เกิดปฏิกิริยาไฮโดรดีออกซิเจนชั้น ในขณะที่การเพิ่มอุณหภูมิส่งผลให้เกิดปฏิกิริยาดีคาร์บอกซิเลชันและดีคาร์บอนิลเลชัน ภาวะที่เหมาะสมในการทำปฏิกิริยา คืออุณหภูมิ 280 องศาเซลเซียส ความดัน 60 บาร์ และเวลา 6 ชั่วโมง พบว่าตัวเร่งปฏิกิริยาซัลไฟด์ของ Ni-Mo ที่อัตราส่วนโดยโมล Ni/(Mo+Ni) เท่ากับ 0.2 เกิดปฏิกิริยาไฮโดรดีออกซิเจนชั้นได้ดีกว่าตัวเร่งปฏิกิริยาซัลไฟด์ของ Co-Mo ที่อัตราส่วนโดยโมล Co/(Mo+Co) เท่ากับ 0.2 แสดงได้จากร้อยละการเปลี่ยนของกรดโอเลอิก (ร้อยละ 100 โดยมวล) ร้อยละการเล็อกเกิด C₁₈ (ร้อยละ 78.8 โดยมวล) และร้อยละผลได้ของ C₁₈ (ร้อยละ 70.3 โดยมวล)



สาขาวิชา ปิโตรเคมีและวิทยาศาสตร์พอลิเมอร์ ลายมือชื่อนิติต

ปีการศึกษา 2560

ลายมือชื่อ อ.ที่ปริกษาหลัก

ลายมือชื่อ อ.ที่ปริกษาร่วม

5772282523 : MAJOR PETROCHEMISTRY AND POLYMER SCIENCE

KEYWORDS: HYDRODEOXYGENATION / OLEIC ACID / UNSUPPORTED
SULFIDE CATALYST / BIO-HYDROGENATED DIESEL

PAPHAWEE SANGGAM: HYDRODEOXYGENATION OF OLEIC ACID
ON UNSUPPORTED Co- Mo AND Ni- Mo SULFIDE CATALYSTS.

ADVISOR: PROF. PATTARAPAN PRASASSARAKICH, Ph. D. , CO-

ADVISOR: BOONYAWAN YOOSUK, Ph.D., 84 pp.

In this research, hydrodeoxygenation (HDO) of oleic acid (model compound of palm oil) over unsupported Co-Mo and Ni-Mo sulfide catalysts was carried out in Parr reactor to produce bio-hydrogenated diesel (BHD). The effects of reaction parameters: temperature, hydrogen pressure and the mole ratio of catalysts ($Ni/(Ni+Mo)$ or $Co/(Co+Mo)$) on the conversion and product yields (mainly n-C₁₇ and n-C₁₈ hydrocarbons) were investigated to find the optimal conditions. The results showed that high pressure favored a HDO pathway, while high temperature strongly affected to decarboxylation and decarbonylation pathways. At optimal condition as temperature of 280°C, reaction times of 6 h and hydrogen pressure of 60 bars, the Ni-Mo sulfide catalysts with Ni/(Ni+Mo) ratio of 0.2 exhibited better performance for the oleic acid HDO than Co-Mo sulfide in term of oleic acid conversion (100 wt%), n-C₁₈ selectivity (78.8 wt%) and n-C₁₈ yield (70.3 wt%).

Field of Study: Petrochemistry and
Polymer Science

Academic Year: 2017

Student's Signature

Advisor's Signature

Co-Advisor's Signature

ACKNOWLEDGEMENTS

The author would like to express their sincere gratitude to Prof. Dr. Pattarapan Prasassarakrich and Dr. Boonyawan Yoosuk for their professional guidance, supervision, and continued support during this graduate studies. The author would also like to extend deep appreciation to members of committee team, Assoc. Prof. Dr. Pranut Potiyaraj, Assoc. Prof. Napida Hinchiranan, and Asst. Prof. Dr. Suwadee Kongparakul for their comments and constructive suggestions.

The author gratefully acknowledges the support of the National Metal and Materials Technology Center (MTEC), the Program in Petrochemistry and Polymer Science and all technicians of the Renewable Energy Laboratory for their help in handling the analytical instruments.

Finally, the author would especially like to thank my parents for their love, valuable support and encouragement throughout my research. Special thanks are expanded to my friends for their friendships and cheerful support.

CONTENTS

	Page
THAI ABSTRACT	iv
ENGLISH ABSTRACT.....	v
ACKNOWLEDGEMENTS	vi
CONTENTS.....	vii
LIST OF TABLES	x
LIST OF FIGURES	xi
CHAPTER 1 INTRODUCTION	1
1.1 The Purpose of the Investigation.....	1
1.2 Objectives	2
1.3 Scopes of the Research Work.....	3
1.4 Expected Outcome.....	4
CHAPTER 2 THEORY AND LITERATURE REVIEWS	5
2.1 Biomass	5
2.2 Palm oil.....	6
2.3 Biodiesel	7
2.3.1 Biodiesel production.....	8
2.3.2 Biodiesel feedstocks	8
2.4 Hydrodeoxygenation (HDO) process	9
2.5 Biomass Catalyst preparation	12
2.5.1 Bulk Catalysts.....	12
2.5.2 Catalyst Supports.....	15
2.6 Catalyst for HDO process.....	16
2.7 Molybdenum disulfide (MoS ₂) Catalyst.....	17
2.7.1 Structures.....	17
2.7.2 Reactivity.....	19
2.7.3 Catalysis	20
2.8 Literature reviews	22
CHAPTER 3 EXPERIMENTAL.....	26

	Page
3.1 Chemicals	26
3.2 Equipments	27
3.3 Procedure	27
3.3.1 Preparation of catalysts	28
3.3.2 Hydrodeoxygenation (HDO) reaction	28
3.3.3 Product analysis.....	28
3.4 Measurements of catalyst performance	29
3.5 Characterization of catalysts.....	30
CHAPTER 4 RESULTS AND DISCUSSION.....	32
4.1 Catalyst characterization	33
4.1.1 X-ray Diffraction (XRD).....	33
4.1.2 N ₂ adsorption-desorption Measurement (BET).....	35
4.1.3 Morphology	39
4.1.4 Temperature-programmed reduction (TPR).....	41
4.2 Hydrodeoxygenation of oleic acid.....	43
4.2.1 Effect of reaction time	43
4.2.2 Effects of temperature and pressure	44
4.2.3 Effects of Ni/(Mo+Ni) and Co/(Mo+Co) mole ratio.....	49
4.2.4 Effect of oleic acid to catalyst ratio.....	53
4.2.5 Comparison of sulfide catalysts on oleic acid HDO	55
4.2.6 Oxygen contents of products and oxygen removal efficiency	57
CHAPTER 5 CONCLUSIONS	58
5.1 Conclusions	58
5.2 Suggestions of the Future Work	59
REFERENCES	60
APPENDIX.....	66
VITA.....	84

LIST OF TABLES

	Page
Table 2.1 Fatty acid content of commercial refined palm kernel oil compared to that of palm olein oil	7
Table 2.2 Main feedstock used for biodiesel production with their respective oil %..	9
Table 3.1 The chemical agents used in this research.	26
Table 4.1 Composition and properties of the MoS-C, MoS-A, Ni-Mo-S-A and Co-Mo-S-A unsupported catalysts with various Ni/(Mo+Ni) or Co/(Mo+Co) mole ratios.....	36
Table 4.2 Physical properties of the MoS-C, MoS-A, Ni-Mo-S-0.2 and Co-Mo-S-0.2.....	39
Table 4.3 Effect of reaction time on hydrodeoxygenation of oleic acid.....	44
Table 4.4 Effects of temperature and pressure on HDO over Ni-Mo-S-0.2 catalyst. 46	46
Table 4.5 Effect of Ni/ (Mo+ Ni) and Co/ (Mo+ Co) mole ratio on HDO over unsupported sulfide catalyst.....	50
Table 4.6 Effect of oleic acid/ catalyst ratio on HDO over unsupported sulfide catalyst	53
Table 4.7 Comparison of sulfide catalysts on oleic acid HDO	55
Table 4.8 Oxygen contents of products and oxygen removal efficiency	57

LIST OF FIGURES

	Page
Figure 2.1 CO ₂ cycles for petroleum and biomass-derived fuels	6
Figure 2.2 Palm oil (a) trees (b) fruit	6
Figure 2.3 The transesterification that produces biodiesel. R ¹ , R ² and.....	8
Figure 2.4 Hydrodeoxygenation of the basic building blocks of biomass to renewable hydrocarbon fuels	10
Figure 2.5 Possible pathway reactions during the conversion of a triglyceride molecule under catalytic hydrotreatment.....	11
Figure 2.6 Catalyst development for hydrodeoxygenation reaction	17
Figure 2.7 (a) Three dimensional representation of the structure of MoS ₂ . (b) Optimized structures of MoS ₂ monolayer with four adsorption sites:(1) hollow site, (2) top site of the S atom, (3) Mo–S bridge site, and (4) top site of the Mo atom.....	18
Figure 2.8 Schematic drawing of common poly-types for MoS ₂	19
Figure 2.9 ‘Rim-edge’ model for catalytic activity of MoS ₂	21
Figure 2.10 Interaction between the Co atoms of the Mo-edge and the S-atoms of the Sedge and repulsion between the Co and Mo atoms of the Mo-edge	22
Figure 3.1 Parr reactor model 4848	27
Figure 4.1 XRD pattern of the MoS-C, MoS-A and unsupported Ni-Mo sulfide catalysts with various Ni/(Mo+Ni)	34
Figure 4.2 XRD pattern of the MoS-C, MoS-A and unsupported Co-Mo sulfide catalysts with various Co/(Mo+Co).....	34
Figure 4.3 N ₂ adsorption/desorption isotherms of the (a) MoS-C and (b) MoS-A...37	

Figure 4.4	N_2 adsorption/desorption isotherms of the (a) Ni–Mo and (b) Co-Mo sulfides of various Ni/(Mo+Ni) or Co/(Mo+Co) mole ratios.	38
Figure 4.5	TEM images of (a) MoS-C, (b) MoS-A, (c) Ni-Mo-S-0.2 and (d) Co-Mo-S-0.2 catalysts	40
Figure 4.6	TPR profiles of the MoS-C, MoS-A, Ni-Mo-S-0.2 and Co-Mo-S-0.2 catalysts.....	42
Figure 4.7	Effect of reaction time on n-C ₁₈ yield.	43
Figure 4.8	Effect of temperature on oleic acid hydrogenation over Ni-Mo-S-0.2 Catalyst, (a) product yield, (b) oleic acid conversion and product selectivity.	47
Figure 4.9	Effect of pressure on oleic acid HDO over NiMo sulfide, (a) product yield, (b) oleic acid conversion and product selectivity.	48
Figure 4.10	Effect of Ni/(Mo+ Ni) mole ratio on product selectivity over NiMo sulfide, (a) product yield, (b) oleic acid conversion and product selectivity.	51
Figure 4.11	Effect of Co/(Mo+Co) mole ratio on product selectivity over CoMo sulfide, (a) product yield, (b) oleic acid conversion and product selectivity.	52
Figure 4.12	Effect of oleic acid/catalyst ratio on product selectivity over NiMo sulfide, (a) product yield, (b) oleic acid conversion and product selectivity.	54
Figure 4.13	Comparison of sulfide catalysts on oleic acid HDO, (a) oleic acid conversion and product selectivity, (b) product yield.....	56

CHAPTER 1

INTRODUCTION

1.1 The Purpose of the Investigation

Currently, the development of renewable fuels from biomass is an important key to future energy due to depleting of the fossil fuels, rising petroleum prices and increasing concern about global warming. Biodiesel is one of the alternative renewable energy as it can reduce un-burnt hydrocarbon and greenhouse gas emissions. Typically, triglycerides are converted via transesterification with methanol to produce fatty acid methyl esters (FAMEs) which commonly referred to as 1st generation biodiesel. However, the use of FAMEs have some drawbacks such as low thermal and oxidative stability, limited compatibility with conventional diesel engine, increased NO_x emissions and possible engine problems due to their higher acid number than that of conventional diesel fuels. To overcome the disadvantages of FAMEs, the catalytic hydrodeoxygenation (HDO) can be applied for biodiesel upgrading process, where the oxygen is eliminated in form of water in presence of hydrogen. This process, triglycerides and fatty acids are converted to straight chain alkane ranging from n-C₁₅ to n-C₁₈ known as middle distillates, which are suitable to use as diesel fuels.

Bio-hydrogenated diesel (BHD), so-called 2nd generation biodiesel, which has a similar molecular structure as petroleum diesel and provides better diesel properties can be produced by the catalytic deoxygenation of triglycerides through three major reaction pathways, including decarbonylation (DCO), decarboxylation (DCO₂), and hydrodeoxygenation (HDO), under reaction conditions of 350–450 °C and 5–15 MPa H₂. There are three types of catalysts most frequently used in hydrotreating of triglycerides: (1) metal catalysts, such as Ni, Pd, Pt, Rh and Ru; (2) bimetallic sulfide catalysts e.g. NiMoS₂, CoMoS₂, and NiWS₂; and (3) metal phosphide and carbide catalysts, e.g., Ni₂P, W₂C, and Mo₂C. For example, Pd/C catalysts were shown to be highly effective in the selective hydrodeoxygenation of ethyl stearate into alkanes. The

hydrodeoxygenation of methyl esters of fatty acids in the presence of a Pt/Al₂O₃ catalyst also leads to a high yield of alkanes. In general, the catalysts based on noble metals are more active, but more expensive. Therefore, catalysts with the active component based on less expensive metals are of greater interest. The conventional catalysts used in HDO process include mainly CoMoS/ γ -Al₂O₃ and NiMoS/ γ -Al₂O₃ because hydrotreating catalysts are less expensive catalysts and known to be active in the sulfide form. γ -Al₂O₃ support has been widely used because of its high surface area and acidic character, but on the other hand, it is unsuitable for HDO, as it is converted to boehmite (AlO(OH)) in the presence of water at elevated temperatures. Al₂O₃ support also showed high tendency for coke deposition caused by polymerization reactions of unstable species on the catalyst surface, so the use of neutral (e.g. carbon) supports or the use of unsupported catalysts with either high surface area or sufficient activity seems promising.

The use of unsupported MoS₂ is advantageous because of its low price and high selectivity towards HDO while some forms of its diverse morphology might result in a high catalytic activity. From previous work, the HDO of palmitic acid using unsupported MoS₂ catalysts with different morphologies was compared with a commercial crystalline MoS₂. This study would focus on hydrodeoxygenation of oleic acid as model compound of palm oil on unsupported Co-Mo and Ni-Mo sulfides prepared by hydrothermal method. The promoter effect on catalyst morphology is also studied. The effects of reaction conditions on the activity and selectivity were investigated. Moreover, the understanding of operating parameters is important to obtain the optimal conditions.

1.2 Objectives

1. To determine the hydrodeoxygenation performance of unsupported Co-Mo and Ni-Mo sulfide catalysts using oleic acid as model compound of palm oil.
2. To study the effects of operating parameters on the activity and selectivity of unsupported Co-Mo and Ni-Mo sulfide catalysts for hydrodeoxygenation.

1.3 Scopes of the Research Work

1. Survey the previous literatures.
2. Prepare the Co- Mo and Ni- Mo sulfide catalysts using ammonium tetrathiomolybdate (ATTM) by hydrothermal method.
3. Characterize the unsupported Co-Mo and Ni-Mo sulfide catalysts.
4. Study the hydrodeoxygenation of oleic acid and analyze the liquid products as follows:
 - Gas chromatography-Mass spectrometry (GC/MS)
 - Gas chromatography with Flame Ionization Detection (GC-FID)
5. Study the effects of operating parameters on the activity and selectivity of unsupported Co-Mo and Ni-Mo sulfide catalysts as follows:
 - Temperature (250, 280, 300 and 320 °C)
 - Hydrogen pressure (20, 40, 60 and 80 bar)
 - Reaction time (1, 3, 6 and 8 h)
 - Oleic acid/catalyst ratio (1.3, 4, 8, 12 and 16 (wt/wt))
 - Mole ratio of catalysts (0.1, 0.2, 0.3, and 0.4)
6. Characterize the unsupported Co-Mo and Ni-Mo sulfide catalysts as follows:
 - The morphology and particle size by transmission electron microscopy (TEM).
 - The surface area, pore size, and pore volume by nitrogen adsorption-desorption measurement.
 - The crystalline phase and structure of catalysts by X-ray diffraction (XRD).
 - The reducibility of catalysts by temperature-programmed reduction (TPR).
7. Summarize the results and write the thesis.

1.4 Expected Outcome

To obtain the optimal conditions of hydrodeoxygenation of the oleic acid and conversion, n-C₁₈ selectivity and n-C₁₈ yield.



CHAPTER 2

THEORY AND LITERATURE REVIEWS

2.1 Biomass

Biomass is a renewable energy source that can be used for the production of fuels and various chemicals. Therefore, biomass and its derivatives have the potential to diversify energy resources and mitigate the environmental impacts. By definition, biomass is biological material derived from living or recently living organisms. From energy point of view, it often refers to plant based material [1]. Biofuel is a renewable energy source produced from biomass and it converts solid, liquid or gaseous fuels. Pyrolysis of a hydrocarbon compound is incomplete thermal degradation in the absence or with low oxygen, which generates a liquid product known as bio-oil [2].

Biomass has the ability to fulfil the basic requirements of performance as the substitute of fossil fuels. Also, from ecological and sustainable points of view, the burning of fossil resources releases a wide variety of undesirable emissions which cause negative environmental impacts and require expensive mitigation processes whereas biomass has negligible content of sulphur and nitrogen and thus, the emissions of SO_x and NO_x are substantially reduced. Furthermore, zero net CO_2 emission from biomass utilization can be achieved due to plant photosynthesis [3].

Typical sources of biomass include, lignin, plant parts, fruits, vegetables, wood chips, chaff, grain, grasses, corn and any cellulose containing biological material or material of biological origin [4]. In contrast to fossil fuels, biomass would be used as a sustainable and renewable energy source due to its contribution for the mitigation of carbon dioxide from the atmosphere through cycles of regrowth and combustion (Figure 2.1).

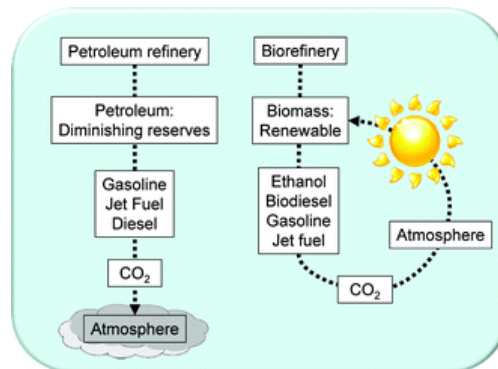


Figure 2.1 CO₂ cycles for petroleum and biomass-derived fuels [5].

2.2 Palm oil

Palm oil is an edible vegetable oil extracted from the mesocarp of the fruit of oil-palm tree (*Elaeis guineensis*) and contains higher level of unsaturated fatty acids with lower in oil-to bunch content [6]. The origin of this type of palm tree can be tracked to a region along the coastal strip of Africa between Liberia and Angola. The tree can be raised in places with abundant rainfalls and heat such as tropical countries in Southeast Asia and South America. Generally, an oil palm tree starts to bear fruit after 3-4 years. The fruit comprises exocarp, mesocarp, endocarp (shell), and endosperm (kernel) as shown in Figure 2.2. The mesocarp and endosperm contains 45-55% edible oil.

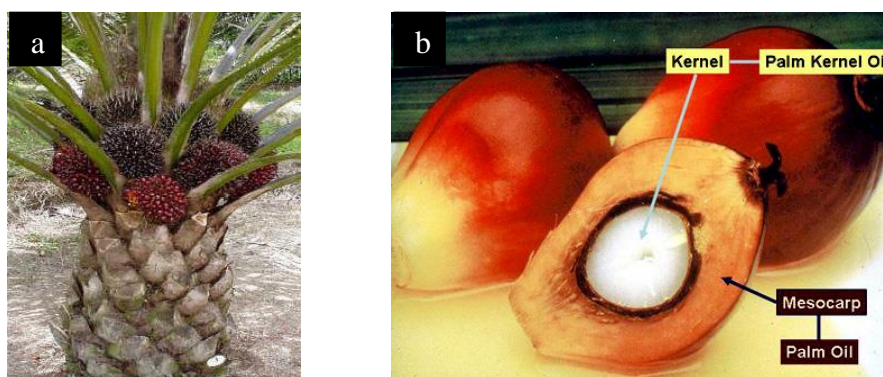



Figure.2.2 Palm oil (a) trees (b) fruit [6].

Palm kernel oil, from the palm seed, is closer in composition to coconut oil than to palm oil. It is more saturated (about 80 percent), contains little monounsaturated fat, and often undergoes harsher chemical processing than palm oil. Fractionated palm kernel oil is made by further processing palm kernel oil to remove the liquid portion, leaving behind even more saturated solids. This oil is often used in energy bars, for example, where it makes the coatings less likely to melt [7]. Fatty acid content of commercial refined palm kernel oil compared to that of palm olein oil is presented in Table 2.1.

Table 2.1 Fatty acid content of commercial refined palm kernel oil compared to that of palm olein oil [8].



Fatty acid	Composition (wt.%)	
	Palm olein oil	Palm kernel oil
C8:0	-	1.2
C10:0	-	2.6
C12:0	0.4	48.8
C14:0	0.8	17.3
C16:0	37.4	-
C16:1	0.2	9.1
C18:0	3.6	2.1
C18:1	45.8	16.1
C18:2	11.1	2.3
C18:3	0.3	0.1
C20:0	0.3	-
C20:1	0.1	0.1

2.3 Biodiesel

Biodiesel generally can be defined as a local-produced alternate fuel for diesel engines that originated from the edible and non-edible oils. Biodiesel can be identified as a clear amber-yellowish liquid with similar viscosity to petroleum diesel. Most of the biodiesel researches have concluded that biodiesel is a nonflammable liquid with higher flash point compared to petroleum diesel.

2.3.1 Biodiesel production

Summarily, trans esterification is the production of one ester from another ester. In the case of biodiesel, this is production of mono-alkyl esters from a vegetable which consists largely of triacylglycerols, i.e., the glycerol esters of long-chain fatty acids, with a low molecular-weight alcohol. As indicated above, methanol is currently the preferred alcohol for this purpose, giving the methyl esters of the plant oil with a fatty acid profile corresponding to that of the parent oil. The transesterification reaction is well-known and is, to a significant extent, textbook material. It can be catalyzed by both acids and bases, with base catalysis being considerably more rapidly. The overall reaction, which is reversible, is shown in Figure 2.3.

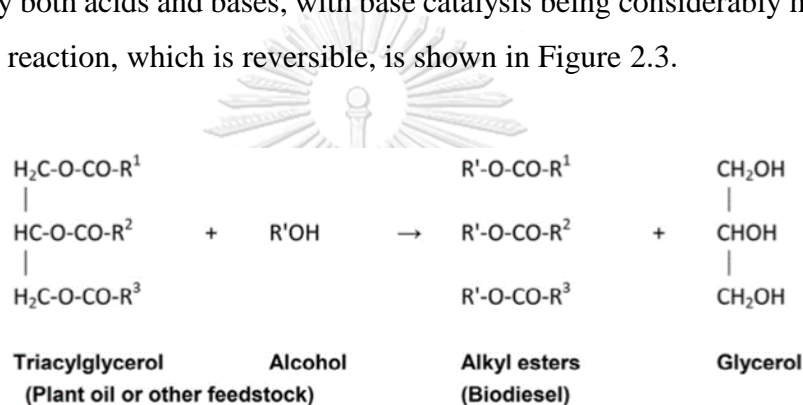


Figure 2.3 The transesterification that produces biodiesel. R^1 , R^2 and R^3 represent different fatty acid chains. R^1 , R^2 and R^3 [9].

2.3.2 Biodiesel feedstocks

The starting materials used for biodiesel production are vegetable oils (or more generally, plant oils) or other oils and fats consisting largely of triacylglycerols. The most common feedstocks in the past and up to the present have been commodity vegetable oils such as rapeseed, palm, soybean and coconut. The issue of expanding the base of feedstocks has led to significant interest in other potential source of triacylglycerol-based oils and main feedstock used for biodiesel production with their respective oil is presented in Table 2.2.

Table 2.2 Main feedstock used for biodiesel production with their respective oil % [10].

Type of oil	Feedstock	Oil content % (w/w)
Edible	Soybean	15–20
	Rapeseed	38–46
	Sunflower	25–35
	Peanut oil	45–55
	Coconut	63–65
	Palm	30–60
Non-Edible	Jatropha seed	35–40
	<i>Pongamia pinnata</i>	27–39
	Neem oil	20–30
	Castor	53
Other sources	Rubber seed	40–50
	Sea mango	54
	Cotton seed	18–25
	Microalgae	30–70

2.4 Hydrodeoxygenation (HDO) process

Hydrotreating process includes hydrodesulphurization (HDS), Hydrodenitrogenation (HDN), hydrodeoxygenation (HDO) and hydrodemetallization (HDM) reactions. These reactions can occur simultaneously during a catalytic hydrotreating process and the extent of these chemical reactions depends on the type of feedstock, chemicals, catalysts and operating conditions of the reaction system. The oxygen content of the bio-based fuel plays a major role in assessing the fuel properties. It is desirable to have a low oxygen content in the fuel. The high oxygen content of vegetable oils (up to 50 wt.%) has adverse effects such as low heating value, thermal and chemical instabilities, corrosivity, immiscibility with fossil fuels and increase in the tendency towards polymerization. Hydrodeoxygenation of the basic building blocks of biomass to renewable hydrocarbon fuels is shown in Figure 2.4.

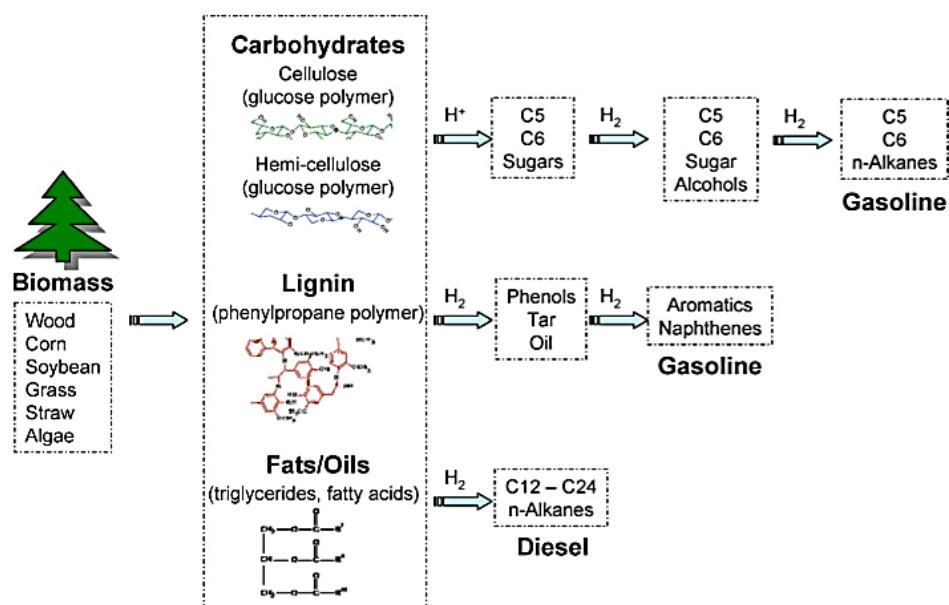
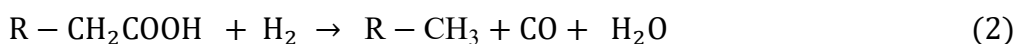
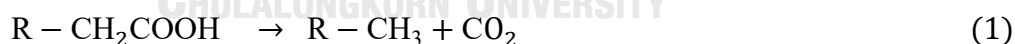


Figure 2.4 Hydrodeoxygenation of the basic building blocks of biomass to renewable hydrocarbon fuels [11].

Hydrotreating of triglycerides through 3 major reaction pathways including decarboxylation, decarbonylation, and hydrodeoxygenation is shown in Equations (1)-(3), respectively.



First, the reaction proceeds via hydrogenation of unsaturated triglycerides (C=C double bond) to form saturated triglycerides, followed by hydrogenolysis of saturated triglycerides resulting in fatty acids and propane. Finally, the fatty acid undergoes through following reactions:

1. Hydrodeoxygenation (HDO), an exothermic reaction, removes oxygen in the form of water and yields n-alkane with same carbon number as the corresponding fatty acid.

2. Decarbonylation (DCO), endothermic reactions, leads to elimination of oxygen in form of CO and water with one carbon atom loss compared to original fatty acid.

3. Decarboxylation(DCO₂), endothermic reactions, leads to elimination of oxygen in form of CO₂. The consequent n-alkane has one carbon atom loss compared to the original fatty acid [12]. Possible pathway reactions during the conversion of a triglyceride molecule under catalytic hydrotreating is shown in Figure 2.5

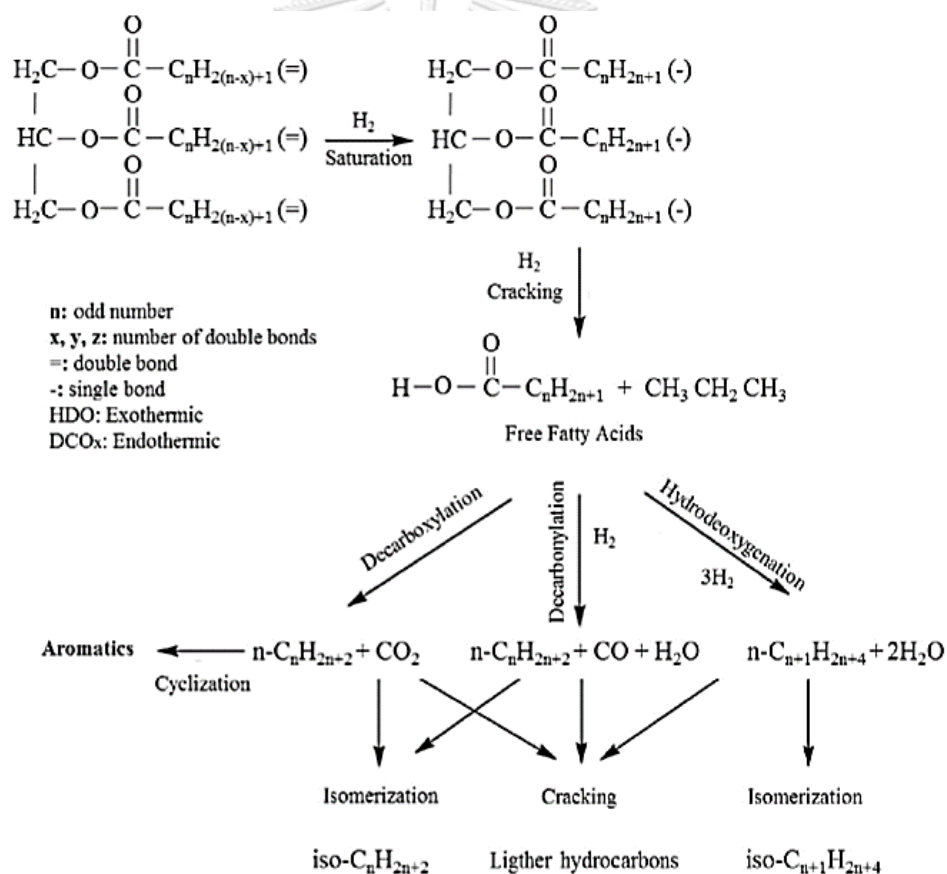


Figure 2.5 Possible pathway reactions during the conversion of a triglyceride molecule under catalytic hydrotreating [13].

2.5 Biomass Catalyst preparation

Catalytic materials can be roughly divided into two families: (1) Bulk catalytic materials and (2) Supported catalytic materials.

Preparation procedures of catalyst powders may differ significantly for supported and unsupported bulk catalysts. However, for most sophisticated materials, several components can be included in catalyst formulations using techniques typical for both supported and bulk materials preparation. In fact, in a typical list of catalytic materials, a number of components can be included. They are:

- (1) The active phase, supposed to be that mainly responsible for the rate determinant catalytic act;
- (2) The support, if needed to produce optimal activity of the active phase and optimal morphology and surface area, with optimization sometimes also of heat transfer and flow-dynamics aspects;
- (3) Promoters that can further improve the catalytic activity

2.5.1 Bulk Catalysts

Bulk catalysts are solids which are largely homogeneous in phase and composition at the spatial level. This is unlike supported catalysts where the catalyst contains a distinct active phase and a “support” or “carrier” component. The primary role of the latter is to provide a substrate with a high surface area for dispersion of the active phase, provide microstructure, mechanical, and thermal resistance to the catalyst. Bulk catalysts encompass a wide variety of materials. These include binary oxides such as alumina, silica and magnesia to transition metal oxides such as chromia, zirconia or titania. The majority of bulk catalysts are prepared from base metals because of their lower costs. Some exceptions are gauze catalysts like Rh, Pt, Pd and their alloys, which are precious metals [14].

The method of preparation of bulk catalysts varies with the type of catalyst. Simple or mixed oxides, and even mixed agglomerated oxide catalysts and heteropoly acids, are prepared largely by precipitation. The sol-gel technique is sometimes used. Zeolites are prepared by hydrothermal synthesis. Sponge metals and alloy catalysts are

prepared by melt alloying (fusion) and quenching. Resins, such as IERs, are prepared by cross linked polymerization.

(a) Precipitation

Precipitation has been the mainstay in the preparation of bulk catalysts because of its ease of practice and also that it is accomplished with relatively simple and inexpensive equipment. The typical steps constitute selection of precursor salts, preparation of a solution of the desired concentration of the solute, precipitation and aging at desired conditions of pH, temperature, and pressure. This is followed by a series of steps which may be common to other methods of preparation as well, such as washing, drying, comminution, shaping, and thermal treatment such as calcinations and activation.

(b) Sol-gel

The sol-gel technique is adopted when there is a requirement for a high degree of control over the textural properties of the material and also the dispersion of components is required at near molecular scale. Materials of high purity can be produced due to the use of precursors with very low impurity concentrations. This technique is widely used in preparing ceramics and thin films.

Sols are suspensions of solid particles in a liquid phase. Their equivalent of particles suspended in a gas phase medium is called aerosol. Liquid particles which are suspended in a gaseous medium are called fog and smoke if these particles are solids. The size of these suspended solid particles ranges between 1 and 1000 nm. They present properties such as Brownian movement.

A gel is a molecule which has reached macroscopic dimensions to a point where it extends throughout the solution. It is characterized by a continuity of both the solid [gel] phase as well as the liquid [sol] phase which it encompasses. And both phases exist in colloidal dimensions. Gels can form as polymeric networks or through the agglomeration of particles or by entanglement of chains. Bonds that hold gels together may be irreversible, as in the case of polymeric gels or reversible, as in the case of particulate gels.

(c) Pyrogenic oxide

Pyrogenic oxides such as SiO_2 , Al_2O_3 , TiO_2 , and ZrO_2 which are commonly used as catalyst supports are also produced by the flame hydrolysis method. In this process a mixture of metal precursors such as metal chlorides, chlorosilanes, and organic siloxanes are vaporized, mixed with hydrogen and oxygen and combusted in a burner. The water formed from the combustion of hydrogen hydrolyses the metal precursors and the high temperature facilitates the further conversion of the hydrolysis products to the oxides. The mechanism of formation of primary particles consists of nucleation followed by growth resulting from subsequent deposition. Further growth to form aggregated structures takes place by coagulation and coalescence. The size of aggregated particles can be controlled by adjusting the residence time in the flame hydrolysis section. Parameters such as flame temperature, oxygen: hydrogen ratio, precursor concentration, and the residence time are used to control the properties of the product.

When compared to oxides formed from the precipitation route, pyrogenic oxides are characterized by high purity, much smaller particle size, spherical shape, and little to internal surface area. Therefore, the specific surface area is highly dependent on the particle size. Pyrogenic silicas are X-ray amorphous, whereas the corresponding aluminas are crystalline. Pyrogenic oxides can be formed into shaped catalyst particles by any of the conventional methods such as spray drying, extrusion, or tableting.

(d) Hydrothermal synthesis

Zeolites-based materials are microporous or mesoporous crystalline materials, widely used as catalysts and adsorbents in refinery and petrochemical processes. These materials have replaced many catalysts for various applications. The type of precursor source of Al and Si in the zeolite synthesis is important as it affects the quality and cost of the zeolite. Common Si precursor sources are precipitated silica, sodium silicate, and silica sol, whereas the Al sources are corresponding sulfate/nitrate/chloride salts and sodium aluminate. In addition, the type of templates, such as organic amines, quaternary ammonium halides and hydroxides strongly influence the crystallization and quality of the zeolite.

2.5.2 Catalyst Supports

Catalyst supports, which are also called as carriers, form an integral part of the catalyst formulation, having myriad functions. Common materials used as carriers are silicas, various forms of alumina, titania, zeolites, magnesia, cordierite, activated carbons, alkaline earth aluminates, SiC, and alundum. Binders are different from carriers. Binders are materials which are used to lend shape to catalyst particles. These are used as additives in relatively small concentrations when the components of a catalyst formulation lack the inherent ability to bind into a formed mass of the desired shape with adequate mechanical strength.

(a) Aluminas

Aluminas are used extensively as supports, binders, as catalysts for the dehydration of alcohols or the hydrolysis of carbonyl sulfide. They are amphoteric in nature. The properties of alumina powders such as microstructure, morphology, acidity, and the ratio of amorphous to crystalline form can be varied over a significantly wide range by changing the method of their preparation. Aluminas can also be prepared by flame hydrolysis. These three methods of preparation leave distinctive characteristics in the end product. Aluminas prepared by the precipitation route have high porosity, but relatively higher impurities such as silica, soda, and iron oxide. Aluminas which are prepared by the alkoxide route tend to be highly pure and have good binder properties. Aluminas prepared by flame hydrolysis have a very small particle size and very little porosity.

(b) Silica

The use of silica as a support for catalysts or as a binder for catalysts is well known. Different types of silica are used either as support/ carrier, as catalyst in combination with other oxides/ active metals, and as binder for catalysts. These materials also find applications in coatings/paints as a matting agent, anti-blocking agent in polymer films, an adsorbent for drying applications, an abrasive agent in dentifrice applications, a filler in rubber, tires, and paper industries. Classification of silica depends on the preparation method adopted and difference in physicochemical

properties. They are classified in following categories; silica sols, silica gels, precipitated silicas, and fumed silicas [15].

2.6 Catalyst for HDO process

There are two types of catalyst mostly use in hydrotreating of triglycerides: (1) metal catalysts, such as Ni, Pd, Pt, Rh, Ru and (2) bimetallic sulfide catalysts e.g. NiMoS₂, CoMoS₂, and NiWS₂ supported on Al₂O₃. The metal catalysts are favorable to DCO and DCO₂, while HDO is dominant in bimetallic sulfide catalysts, except NiWS₂. Some metal catalysts such as Ni, Pd, and Pt strongly promoted methanation reaction, consuming large amount of hydrogen. Moreover, using NiMoS₂ and CoMoS₂ as catalysts with good selectivity to HDO can be operated at lower temperature due to the nature of exothermic reaction. The formation of CO and CO₂ could affect product yield, catalyst deactivation, and downstream process for recycle gas. Therefore, using bimetallic sulfide catalysts as NiMoS₂, which was high and selective to HDO, was very attractive for hydrotreating process.

The effects of hydrotreating parameters when using bimetallic sulfide catalysts were explored in various literatures. The results indicated that the temperature, WHSV/LHSV, hydrogen pressure, and H₂/oil ratio as significant operating parameters could alter the reaction pathways in hydrotreating process. Furthermore, the relative activities of the DCO/DCO₂ and HDO reactions, as the most important key in hydrotreating process, were considered to evaluate hydrogen consumption, product yield, heat balance, and catalyst deactivation. However, many researchers estimated the relative activities of the DCO/DCO₂ and HDO reactions using the ratio of the amounts of n-alkanes with odd numbers of carbon atoms, to n-alkanes with even numbers of carbon atoms in the liquid product. These estimations could not provide an actual relative contribution of HDO and DCO/DCO₂ reactions compared to mole balance analysis [16]. Consequently, a comprehensive understanding the influence of reaction parameters on 3 major reaction pathways by using mole balance analysis is crucial. Catalyst development for hydrodeoxygenation reaction is shown in Figure 2.6

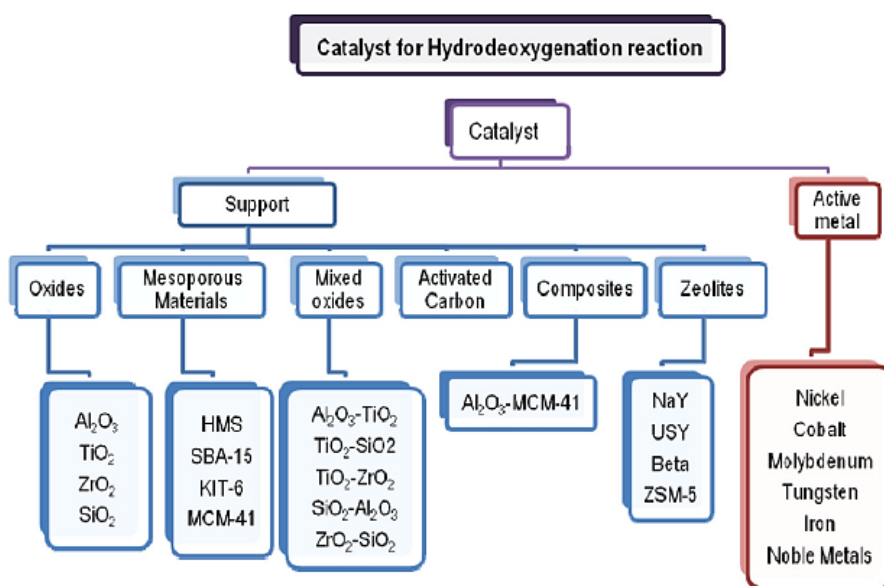


Figure 2.6 Catalyst development for hydrodeoxygenation reaction [17].

2.7 Molybdenum disulfide (MoS₂) Catalyst

2.7.1 Structures

Molybdenum disulfide (MoS₂) has a crystal structure consisting of weakly coupled layers of S-M-S, where a Mo atom layer is sandwiched between two layers of S atoms. It offers a large direct bandgap found experimentally to be around 1.8 eV. Crystals of MoS₂ are composed of vertically stacked, weakly interacting layers held together by van der Waals interactions (Figure 2.7a). As seen in the Figure, the neighboring planes in bulk MoS₂ are held together by weak van der Waals forces, making it possible to produce monolayers of MoS₂ using the well-established micromechanical cleavage and liquid exfoliation techniques.

A single layer, 6.5 Å thick (Figure 2.7a), was extracted using scotch tape or lithium-based intercalation. Figure 2.7b depicts the covalently bonded S-Mo-S unit cell of MoS₂ arranged in a hexagonal lattice with each sulfur atom coordinated with three molybdenum atoms within a single layer of MoS₂. The Mo-S bond is 2.42 Å in

length and the optimized lattice constant of MoS₂ monolayer is 3.18 Å in thickness, which is consistent with the many previous predictions. The adsorption of ad-atoms is a widely used and efficient way to introduce new functionalities in nanoscale applications. The different added atoms used C, B, Au, Mo, Cr, Pt, Pd, Ag, Rh, Ti, Fe, Co and Ni in 10 transition-metal elements (such as Co, Cr, Fe, Mn, Ni, Pt, Sc, Ti, V, and W) to determine ones that can induce magnetization in nonmagnetic 1H-MoS₂. Four typical adsorption sites are observed: (1) the hollow site in the hexagon center, (2) top site of a Mo atom, (3) top site of an S atom, and (4) the bridge site between S Mo bond as shown in Figure. 2.7b. The equilibrium adsorption sites of these 10 atoms were determined by first placing them at one of four different adsorption sites and subsequently optimizing the whole structure

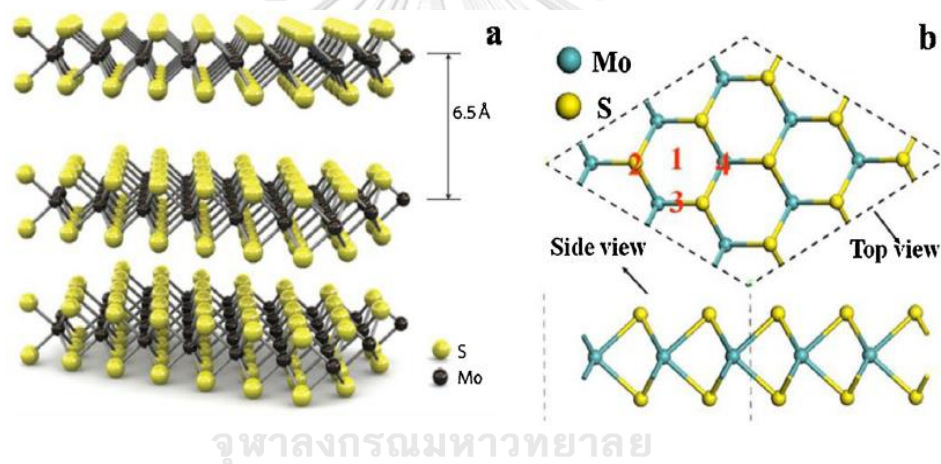


Figure 2.7 (a) Three dimensional representation of the structure of MoS₂. (b) Optimized structures of MoS₂ monolayer with four adsorption sites:(1) hollow site, (2) top site of the S atom, (3) Mo–S bridge site, and (4) top site of the Mo atom [18].

Four poly-types of MoS₂ have been described. They are 1T MoS₂, 1H MoS₂, 2H MoS₂ and 3R MoS₂. Of these, the 1H phase is the most stable among all poly-types, and the 1T MoS₂ and 3R MoS₂ are meta-stable. Schematic drawing of these common poly-types for MoS₂ is shown in Figure 2.8

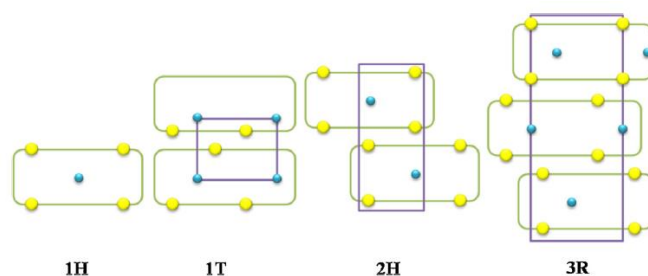


Figure 2.8 Schematic drawing of common poly-types for MoS₂ [19].

The 1T MoS₂ has the molybdenum atoms coordinated octahedrally by the sulfur atoms to form a unit cell; 1H phase (the basic unit of MoS₂ monolayer) has the molybdenum atoms coordinated octahedrally by the sulfur atoms and sandwiched in the form of S- Mo- S; 2HMoS₂ has trigonal prismatic coordination around the molybdenum atom with two S-Mo-S units per elemental cell; the 3R MoS₂ also has the same trigonal prismatic coordination as the 2H MoS₂ but with three S- Mo- S units per elemental cell along the c-axis direction [20]. In the case of lithium deposition on a single crystal of MoS₂ at room temperature, the lithium atom is intercalated into the MoS₂. Two reactions take place: (a) an intercalation reaction according to the rigid band model and (b) an intercalation reaction accompanied by a phase transition from 1H or 2H to 1T. This transformation is caused by the electron transfer from the alkali metal to the d orbital of the transition metal center, which results in the metallic-like character of the material and causing destabilization of the lattices related to the diffusion of the lithium atom.

2.7.2 Reactivity

MoS₂ may act in the intercalation processes as a reservoir of both electric charge and chemical species. Nevertheless, this sulfide behaves as a rather chemically inert substance. Thus, etching using a standard solution of hydrochloric acid, nitric acid, or sulfuric acid leads to very rare or no incidence of holes on the surface after a normal etching time. Only a solution of sulfuric acid with potassium dichromate was found to create large and deep defects on the MoS₂ (001) faces. Resistance against

photocorrosion in solution, useful for photoelectrochemical applications, has also been observed. Such a feature was originally attributed to the fact that the optical transition responsible for the creation of the electron–hole pairs is between non-bonding metal d states [21]. However, later detailed band structure calculations have shown that in these chalcogenides the relevant state at the top of the valence band is not a non-bonding metal d state, but rather an antibonding state between metal d_z^2 and non-metal p_z orbitals. This antibonding character is believed to be responsible for the high stability of this material against photocorrosion.

2.7.3 Catalysis

The catalytic properties of the molybdenum sulfide are, as mentioned above, closely related to the structural properties of the material. Research in this area has focused mainly on two kinds of processes: dark electron transfer processes as hydrogenation activity and hydrogen evolution; and photochemical processes. Electrochemical studies show that the former occurs in the absence of light at centers located in the plane parallel to the c -axis, while the photoreactions occur on the van der Waals planes. This is probably because the contributions of the non-bonding orbitals d_z^2 or antibonding d_z^2 – p_z orbitals, forming the valence band, are located toward the van der Waals surface, while the orbitals which form the conduction band (dx^2-y^2 , d_{xy} , d_{xz} , d_{yz} and np_y) are oriented towards the surface parallel to the c -axis. High-activity catalysts are achieved when the single molecular layers of MoS_2 , deposited onto a high surface area and doped with a nickel salt, is calcinated and reduced. However, the most active species appears to be an oxysulfide. Even in the absence of nickel as the promoter, the catalysts prepared by exfoliation show activities which are at least comparable to those prepared by precipitation from ammonium heptamolybdate.

The knowledge about the nature and position of the active sites in MoS_2 -based catalysts has been an important problem for many years. A cluster approach of active sites in MoS_2 catalysts using differential functional theory (DFT) calculations has been reported [22]. Most stable configuration corresponds to a flat absorption of a molecule of thiophene on the edge of the MoS_2 sheet. An interesting approach is the ‘rim-edge’ site model in which the MoS_2 catalyst particle is described as a stack of several discs.

There, the activity of unsupported MoS₂ is related to the coexistence of two different sites, which are directly dependent on the morphology of the MoS₂ crystallites, and more precisely, on the stacking height of the layers (see Figure 2.9). The hydrogenation reaction is found to be catalyzed predominately by rim sites, while edge sites catalyze sulfur removal. The nature of the MoS₂—pristine, exfoliated or delaminated—would be certainly important for determining the catalytic activity of this material. In fact, MoS₂ in alumina-supported catalysts obtained by conventional preparation techniques is mostly formed by the single layer sheets [58]. Supported single layer MoS₂, prepared by the exfoliation of Li_xMoS₂ and deposited on γ -alumina, is stable under the hydrodesulfurization reaction conditions, showing catalytic activity and selectivity similar to those of an alumina-supported multilayer MoS₂ catalyst.

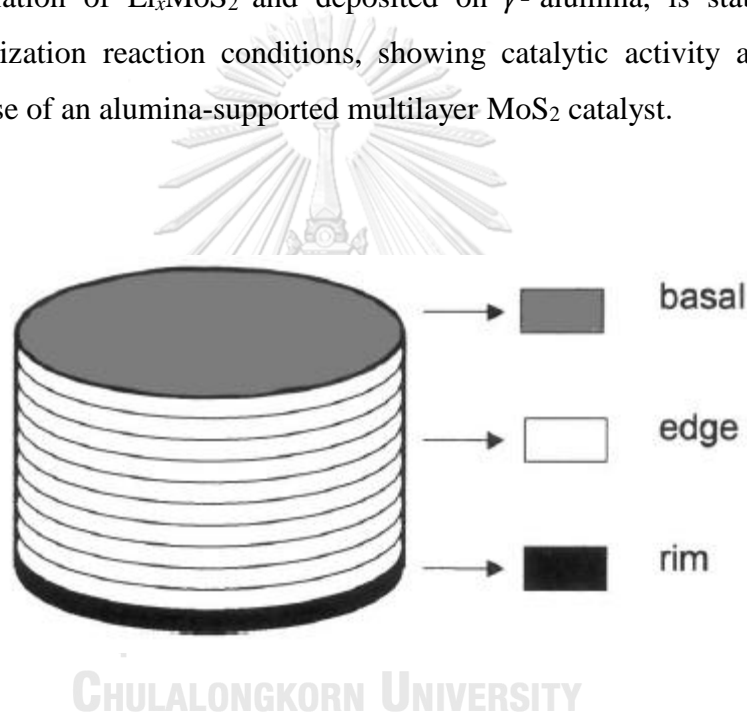


Figure 2.9 ‘Rim-edge’ model for catalytic activity of MoS₂ [16].

An intermediate structure formed on the Mo-edge contains weakly bonded Co atoms. In this state the Co atoms are affected by the repulsion from the Mo atoms of the Mo-edge and the attraction by the S atoms of the neighboring S-edge (Figure 2.10). As a result, Co-S bonds break and Co atoms move from the Mo-edge to the fully sulfidized S-edge. After the elimination of hydrogen from the S-edge (possibly into the gas phase, or onto a carrier, or onto neighboring edges) and rebuilding of the Mo-edge (step 2) the S-edge promoted by Co atoms, interacts with gas phase hydrogen (step 3). At this stage the Mo-edge is partly reduced (sulfidation state is about 50%), whereas

the S-edge is fully sulfidized. The interaction of molecular hydrogen with the S-edge proceeds similarly to the interaction of the H₂ with the Mo-edge (Scheme 1) through the heterolytic dissociation of the H₂ molecules on sulfur atoms of the S-edge and the formation of hydride hydrogen on Co atoms. Energetic expediency of a similar process for NiMoS catalyst was, recently proved by Weber and van Veen by quantum chemical computations [23]. After electron transfer hydride hydrogen changes its electric charge and moves to the SH group forming H₂S on the S-edge.

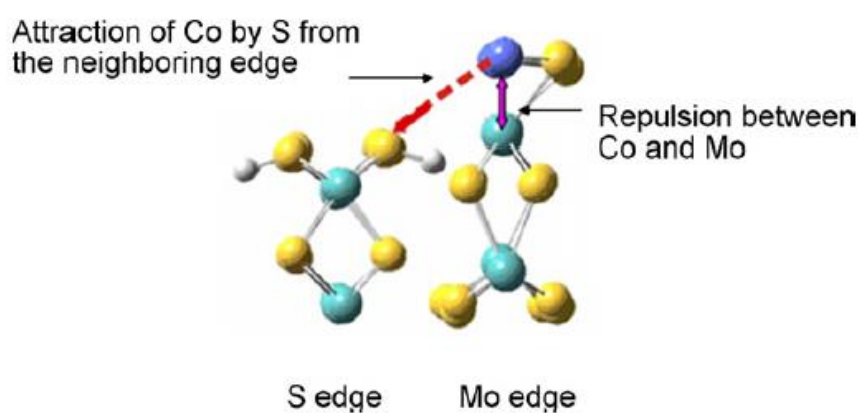


Figure 2.10 Interaction between the Co atoms of the Mo-edge and the S-atoms of the Sedge and repulsion between the Co and Mo atoms of the Mo-edge [24].

2.8 Literature reviews

Yoosuk et al. [25] studied the effect of Co and Ni on the hydrodesulfurization (HDS) activity of unsupported Mo sulfide catalysts prepared by hydrothermal method using ammonium tetrathiomolybdate (ATTM) for the simultaneous HDS of dibenzothiophene (DBT) and 4,6-dimethyldibenzothiophene (4,6-DMBT). The promoter effect on catalyst morphology is also investigated. The result showed that the hydrothermal synthesis using water and organic solvent was found to produce highly active Mo based sulfide nanosize particles. The liquid-phase adsorption showed that different sulfides exhibit different adsorption capacity a selectivity towards 4,6-DMBT and DBT, which reflect on the differences in adsorption sites on the catalyst surface.

The addition of Co or Ni promoter not only increased the catalytic activity of unsupported Mo sulfide catalysts but also changed the contribution of direct-disulfurization and hydrogenation pathways. HDS activity of the unsupported Mo based sulfides was much higher than that of the sulfided commercial Co(Ni)Mo/Al₂O₃ catalysts.

Yoosuk et al. [26] studied the activity and substrate specificity of unsupported amorphous MoS₂ (Mo-A) and compared with a commercial crystalline MoS₂ (Mo-C) for hydrodeoxygenation reaction using phenol as model reactant. The structure and promoter effect of unsupported MoS₂ is evaluated. The unsupported MoS₂, with amorphous and highly bent multi-layer structures, was much active than the highly crystalline structured MoS₂ and resulted in direct oxygen elimination. The enhanced catalytic activity observed with the promoter addition was essentially due to the enhancement of rate of direct-deoxygenation route. The activity and selectivity for phenol HDO can be controlled by morphology and the promoter of the unsupported MoS₂ catalysts.

Srifa et al. [27] investigated the effect of reaction parameters on hydrotreating of palm oil to bio-hydrogenated diesel over NiMoS₂/γ-Al₂O₃. The recommended conditions were as follow: temperature 300 °C, pressure 30-50 bar, LHSV: 1⁻² h⁻¹, and H₂/oil ratio: 750-1000 N (cm³/cm³) with the product yield of 90.0% and n-alkane content > 95.5%. Temperature strongly affected reaction pathway (decarbonylation, decarboxylation, hydrodeoxygenation, cracking and isomerization), while higher pressure promoted hydrodeoxygenation reaction. The increase LHSV suppressed reactions due to the insufficient contact time. H₂/oil ratio should be higher than 3-5 time of theoretical requirement, Furthermore, methanation reaction impacted on H₂ consumption at low temperature and high pressure.

Kiatkittipong et al [28] investigated the suitable operating condition for the hydroprocessing of different palm oil feedstock i.e. crude palm oil (CPO), degummed crude palm oil (DPO) and palm fatty acid distillate (PFAD) over commercial 5 wt% Pd/C and synthesized NiMo/γ-Al₂O₃. The results showed that removal of phospholipid gum from palm oil is beneficial for the hydroprocessing as higher diesel yield could be obtained at milder condition. The highest diesel range product yield of 81% could be obtained from PFAD catalyzed by Pd/C with less severe operating condition (lower

operating temperature and pressure, shorter residence time) than the others. Pd/C catalyst showed good catalytic activity for fatty acid feedstocks but became less promising for triglyceride feedstocks when compared to NiMo/ γ -Al₂O₃.

Toba et al. [29] examined hydrodeoxygenation of low-grade waste oil and clarified catalytic performance and properties of product oils. Low-grade waste oils such as waste cooking oil and trap grease were completely converted into hydrocarbons more than 300 °C. NiMo and NiW catalysts were more suitable for hydrodeoxygenation of low-grade waste oils than CoMo catalyst to prevent the formation of olefin. NiW catalyst gave more hydrocarbons formed by decarboxylation or decarbonylation than NiMo and CoMo catalysts. The sulfur content in the product oil was low when catalytic activity showed content.

Ayodele et al. [30] prepared nickel II oxalate complex (NiO_x) by functionalization of nickel with oxalic acid (O_xA) and incorporated into Al₂O₃ to synthesize alumina supported nickel oxalate (NiO_x/Al₂O₃) for the hydrodeoxygenation (HDO) of oleic acid (OA) into biofuel. The catalytic activity of NiO_x/Al₂O₃ on the HDO of OA produced a mixture of 21% iso-C₁₈ and 72% n-C₁₈ at 360 °C, 20 bar, 30 mg NiO_x/Al₂O₃ loading pressure and gas flow rate of 100 mL/min. The presence of i-C₁₈ was ascribed to the O_xA functionalization which increased the acidity of NiO_x/Al₂O₃. The NiO_x/Al₂O₃ reusability study showed the consistent HDO ability after 5 runs.

Shim et al. [31] studied the effect of Co/Mo ratio on the catalytic performance and related to the activity results in decarboxylation. The catalytic performance of non-sulfide unsupported CoMo catalyst depends on the Co/Mo ratio. Co_{0.5}Mo_{0.5} catalyst exhibits the highest oleic acid conversion, C₁₇ selectivity, and oxygen removal efficiency. Decarboxylation is the main reaction pathway in inert condition. Co_{0.5}Mo_{0.5} catalyst can be promising decarboxylation catalyst for the biodiesel upgrading process.

Nikulshin et al. [32] elucidated the effect of coating alumina by carbon on the catalytic properties of CoMoS catalysts supported on carbon-coated alumina (CCA) in hydrodeoxygenation (HDO) reaction. Using CCA supports instead of alumina for preparation of CoMo catalysts resulted in improving their activities in HDO of guaiacol and oleic acid and significantly reduced deactivation. Enhanced catalytic properties of CoMo/C_x/Al₂O₃ catalyst were related to lower acidity of CCA supports. CoMo/CCA

catalyst with 2 wt% of carbon had maximal activity in HDO of guaiacol and oleic acid thank to an optimal balance between cobalt content into CoMoS phase particles and their average length.

Kubicka et al. [33] focused on investigation of the activity and selectivity of sulfide Ni/ Al₂O₃, Mo/ Al₂O₃ and NiMo/ Al₂O₃ prepared by impregnation in deoxygenation of rapeseed oil. The activity of the catalysts decreased in order NiMo/Al₂O₃ > Mo/Al₂O₃ > Ni/Al₂O₃. The bimetallic NiMo catalysts showed the higher yields of hydrocarbons than the monometallic catalyst at a given conversion. The effect of Ni/(Ni+Mo) atomic ratio to the range 0.2-0.4 on the activity and selectivity was not significant.

Miao et al. [34] demonstrated hydrothermal catalytic deoxygenation of palmitic acid to produce paraffin over a Ni/ZrO₂ catalyst with no or low-pressure (100 psi) external supply of H₂. The results show that the presence of water greatly improved conversion of palmitic acid and paraffin yield. Significant improvement was attributed to the formation of in-situ H₂. Without an external H₂ supply, a 64.2 C% conversion of palmitic acid was achieved in the presence of water, while only a 17.2 C% conversion was achieved without water. The presence of water suppressed the side reaction of palmitic acid, specifically ketonization and esterification. The hydrothermal catalytic process is promising approach for producing liquid paraffin (C₈-C₁₅) from fatty acids under no or low-pressure H₂.

CHAPTER 3

EXPERIMENTAL

3.1 Chemicals

The chemical agents used in this research are presented in Table 3.1

Table 3.1 The chemical agents used in this research.

Chemical agents	Company
Ammonium tetrathiomolybdate (ATTM)	Sigma-Aldrich Co., Ltd. (USA)
Nickel(II) nitrate hexahydrate	Sigma-Aldrich Co., Ltd. (USA)
Cobalt(II) nitrate hexahydrate	Sigma-Aldrich Co., Ltd. (USA)
Oleic acid (99.99%)	Sigma-Aldrich Co., Ltd. (USA)
n-Decane	Sigma-Aldrich Co., Ltd. (USA)
Molybdenum(IV) sulfide	Sigma-Aldrich Co., Ltd. (USA)
Methyl heptadecanoate	Sigma-Aldrich Co., Ltd. (USA)
Carbon disulfide	Sigma-Aldrich Co., Ltd. (USA)
Decahydronaphthalene (decalin)	Fluka Co., Ltd. (Switzerland)
Hydrogen gas (99.99%)	Praxair Co., Ltd. (Thailand)
Iso-propanol	RCI Labscan Co., Ltd. (Thailand)

3.2 Equipments

The equipments used in this research are follows:

- (1) Breaker 50, 100 and 250 ml
- (2) Cylinder 25 and 100 ml
- (3) Paper filter no.42
- (4) Buchner funnel
- (5) Suction fask
- (6) Glass plate
- (7) Parafilm
- (8) Aluminum foil

3.3 Procedure

In this research, the hydrodeoxygenation (HDO) of oleic acid and catalyst preparation were carried out in Parr reactor (Parr reactor model 4848, Parr instrument company (USA)).



Figure 3.1 Parr reactor model 4848

3.3.1 Preparation of catalysts

The Co-Mo or Ni-Mo sulfide catalyst were synthesized by using a step hydrothermal method. The catalysts synthesis was carried out in 250 mL Parr reactor. ATTM (0.15 g) was dissolved in 25 g of deionized water. Then, 2.5 g of organic solvent (decalin) added to this solution. $\text{Ni}(\text{NO}_3)_2 \cdot 6\text{H}_2\text{O}$ or $\text{Co}(\text{NO}_3)_2 \cdot 6\text{H}_2\text{O}$ was dissolved in minimum amount of water and the desired amount of cobalt or nickel was added so as to give the indicated atomic ratio of $\text{Ni}/(\text{Ni}+\text{Mo})$ or $\text{Co}/(\text{Co}+\text{Mo})$ as 0.1, 0.2, 0.3, and 0.4. The reactor was purged, then pressurized with hydrogen gas to an initial pressure of 28 bar and heated to 350 °C. After 1 h, the resulting catalysts were separated and immersed under an organic solvent. Each catalysts was designated as 'Co-Mo-S-X' or 'Ni-Mo-S-X' where X represents the mole ratio of $\text{Ni}/(\text{Ni}+\text{Mo})$ or $\text{Co}/(\text{Co}+\text{Mo})$.

The Mo sulfide catalyst (Mo-S) was prepared by the same procedure as Co-Mo or Ni-Mo sulfide catalyst, but without the Ni or Co precursor. For Ni sulfide catalyst (Ni-S) or Co sulfide catalyst (Co-S) was followed without the addition ATTM except CS_2 use as the sulfur source for nickel or cobalt.

3.3.2 Hydrodeoxygenation (HDO) reaction

The HDO of oleic acid was carried out in 250 mL Parr reactor. The reactor was charged with oleic acid (0.3 g), n-decane (19.7 g) and catalyst (0.075 g), purged with hydrogen gas and then pressurized up to initial pressure of 60 bar. The reactor was heated to 280 °C and maintained at this temperature for 6 h with stirring at 300 rpm. The reactor was then cooled down to room temperature, the gas inside was vented, and the liquid products were rinsed from the reactor. The resulting suspension was filtered under vacuum through Whatman No.42 filter paper to recover the catalysts.

3.3.3 Product analysis

The liquid products after separation were identified by GC/MS (Agilent 7000C GC/MS Triple Quad) with HP-INNOWAX column (30 m x 0.25 mm x 0.25 μm). 0.2 μL of liquid sample was injected into GC with split ratio of 20. The injection and detector temperatures were 225 °C. The temperature program was increased from 60 °C to 250 °C at a rate of 10 °C/min for 5 min and maintained at 250 °C for 15 min.

The liquid products were quantitatively analyzed by GC-FID (Shimadzu 2010) with DB-1 column (60 m x 0.25 mm x 0.1 μ m). 1 μ L of liquid sample was injected into GC with split ratio of 100. The injection and detector temperatures were 325 $^{\circ}$ C. The temperature program was increased from 50 $^{\circ}$ C to 120 $^{\circ}$ C at a rate of 10 $^{\circ}$ C/min, and followed by increase of 5 $^{\circ}$ C/min to 250 $^{\circ}$ C for 5 min.

3.4 Measurements of catalyst performance

a) Response Factor (R_{x_i})

$$R_{x_i} = \frac{M_{int}}{M_i} \times \frac{\text{Peak area of } i}{\text{Peak area of internal standard}} \quad (3.1)$$

where i is the standard, M_i is the amounts of the standard (g), and $M_{\text{internal standard}}$ is the internal standard (g) determined by GC-FID.

b) Amount of reactant or product after HDO reaction (W_i , wt%)

$$W_i = \frac{1}{R_{x_i}} \times \frac{W_{int}}{W_{\text{sample}}} \times \frac{\text{Peak area of } i}{\text{Peak area of internal standard}} \times 100 \quad (3.2)$$

where i is the reactant or product. W_{int} and W_{sample} are the weights of the internal standard and liquid sample (g)

c) Conversion (wt%)

$$\text{Conversion} = \frac{C_{\text{in Feed}} - W_i}{C_{\text{in Feed}}} \times 100 \quad (3.3)$$

where $C_{\text{in feed}}$ is the concentration of reactant in feed (wt%) and W_i is the amount of reactant after reaction (wt%)

d) Selectivity (wt%)

$$\text{Selectivity} = \frac{W_i}{\sum W_i} \times 100 \quad (3.4)$$

where W_i is the amount of n-alkane in product and $\sum W_i$ is the total of amount n-alkane in all products determined by GC-FID (wt%)

e) Yield (wt%)

$$\text{Yield} = \frac{W_i}{\text{Concentration of reactant}} \times 100 \quad (3.5)$$

where W_i is the amount of n-alkane in product determined by GC-FID (wt%).

f) n-Alkane contents (wt%)

$$\text{n-alkane contents} = \sum \text{Yield} \quad (3.6)$$

where $\sum \text{Yield}$ is the total yield in product (wt%).

จุฬาลงกรณ์มหาวิทยาลัย
CHULALONGKORN UNIVERSITY

3.5 Characterization of catalysts**3.5.1 Transmission electron microscopy (TEM)**

The surface morphology of catalysts was studied by TEM using a FEI-TECNAI G² S-Twin transmission electron microscope. A small amount of sample was ground with a mortar and pestle. The sample was suspended in ethanol and sonicate. A drop of the suspension was put on a layer carbon film supported by a Cu grid.

3.5.2 X-ray diffraction (XRD)

The X-ray diffraction patterns were obtained on a X-ray diffractometer/ Bruker AXS-D8 Discover with Cu K α emission, 40 mA 40 kV with a scanning speed of 0.02°/min. The diffractograms were analyzed using the standard JCPDS files.

3.5.3 Nitrogen adsorption-desorption measurements (BET method)

The N₂ adsorption and desorption isotherms were measured on a Micromeritics ASAP 2064 / ASAP 2060 instrument. Pore size distributions of the sample were determined from the isotherms by the Barrett-Joynor-Hallenda (BJH). Fresh catalyst samples were vacuum dried before the adsorption measurement.

3.5.4 Temperature-programmed reduction (TPR)

Temperature programmed reduction was conducted with a BELCAT- B instrument. About 0.1 g of sample was charged in the reactor and heated up to 500 °C at rate of 10 °C / min, held at 500 °C for 30 min and then cooled down to room temperature under Ar flow to remove the absorbed material. A mixture of 4.8 vol% H₂/Ar was introduced at 50 mL/min into sample loop. The heat treated sample was again heated at a rate of 10 °C/min to 650 °C and the effluent gas was passed through a cold viscous solution of isopropanol (Cooled by liquid N₂) to remove the water produced during the reduction reaction and analyzed using thermal conductivity detector.

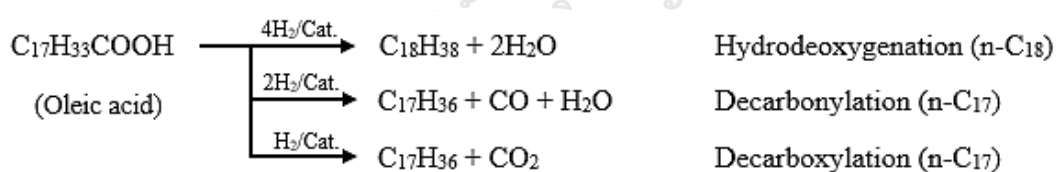
CHAPTER 4

RESULTS AND DISCUSSION

For the experiments using oleic acid ($C_{17}H_{33}COOH$) as feedstock, the performance of unsupported Ni-Mo and Co-Mo sulfide catalysts was compared in terms of oleic acid conversion, product yield, selectivity and oxygen removal. The conversion of oleic acid was calculated from GC-FID data.

The unsupported Co-Mo and Ni-Mo sulfide catalysts were characterized by X-ray diffraction (XRD), nitrogen adsorption-desorption measurements, transmission electron microscopy (TEM) and temperature-programmed reduction (TPR).

Scheme 4.1 shows the deoxygenation pathway of oleic acid. According to the literature, hydrodeoxygenation (HDO) as major pathway removes oxygen in the form of water and yields generally n-alkane with same carbon number as the corresponding fatty acid. On the other hand, decarbonylation (DCO) and decarboxylation (DCO₂) pathways lead to elimination of oxygen in form of CO and CO₂, respectively. The consequent n-alkane has one carbon atom loss compared to the original fatty acid.



Scheme 4.1 Reaction scheme for the HDO of oleic acid on sulfide catalyst [34].

4.1 Catalyst characterization

4.1.1 X-ray Diffraction (XRD)

The XRD patterns of unsupported Mo sulfide catalysts before and after addition of promoters are shown in Figure 4.1 and Figure 4.2. As compared to a commercial MoS₂ powder, both unpromoted and promoted Mo sulfide catalysts exhibit weak XRD peaks, indicating a very poorly crystalline structure characteristic of the molybdenum disulfide. The XRD peaks became broader when the (Ni or Co) promoter was added. The intensity of most MoS₂ peaks were significantly decreased and particularly for the unsupported CoMo sulfide, the peak at $2\theta = 14.4^\circ$, characteristic of the (0 0 2) basal planes of crystalline MoS₂ became very low. In the sulfides with promoters, the diffractions of separated Ni and Co sulfides were detected due to high loading amount of these metals and the crystallized Ni₃S₄ and Co₉S₈ were formed. Yoosuk et al. [35] reported that the catalyst with the Ni/(Mo+Ni) ratio of 0.33 showed the diffraction peaks of poorly crystalline MoS₂, indicating that the MoS₂ maintains its structure in the presence of amorphous Ni.

For the catalysts with the Ni/(Mo+Ni) ratio above 0.2 (Figure 4.1), the diffraction peaks of the second metal sulfide appeared progressively. Ni₃S₄ and NiS were detected in the catalysts with the Ni/(Mo+Ni) ratio of 0.2, 0.3 and 0.4. In most cases, the ternary Mo-Ni-S phase did not appeared clearly. It probably due to the fact that there is overlapping of diffraction peaks from MoS₂ and Mo-Ni-S phase. In the same way, the catalysts with the Co/(Mo+Ni) ratio above 0.2 (Figure 4.2), Co₉S₈ and Co₄S₃ were detected in the catalysts with the Ni/(Mo+Ni) ratio of 0.2, 0.3 and 0.4. For the promoted sulfide catalysts, the Ni-Mo-S or Co-Mo-S phases were not reflected by any major XRD peaks. The active structure (Ni-Mo-S or Co-Mo-S phase) possibly presents as small nano-sized particles, which cannot be detected by XRD method [36].

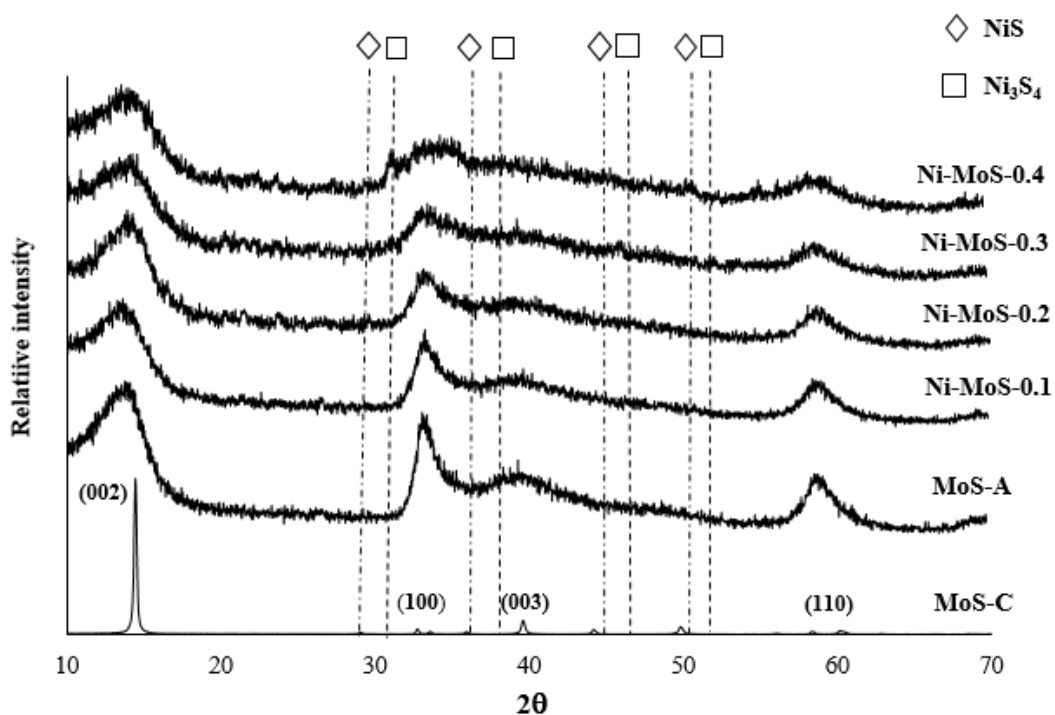


Figure 4.1 XRD pattern of the MoS-C, MoS-A and unsupported Ni-Mo sulfide catalysts with various Ni/(Mo+Ni)

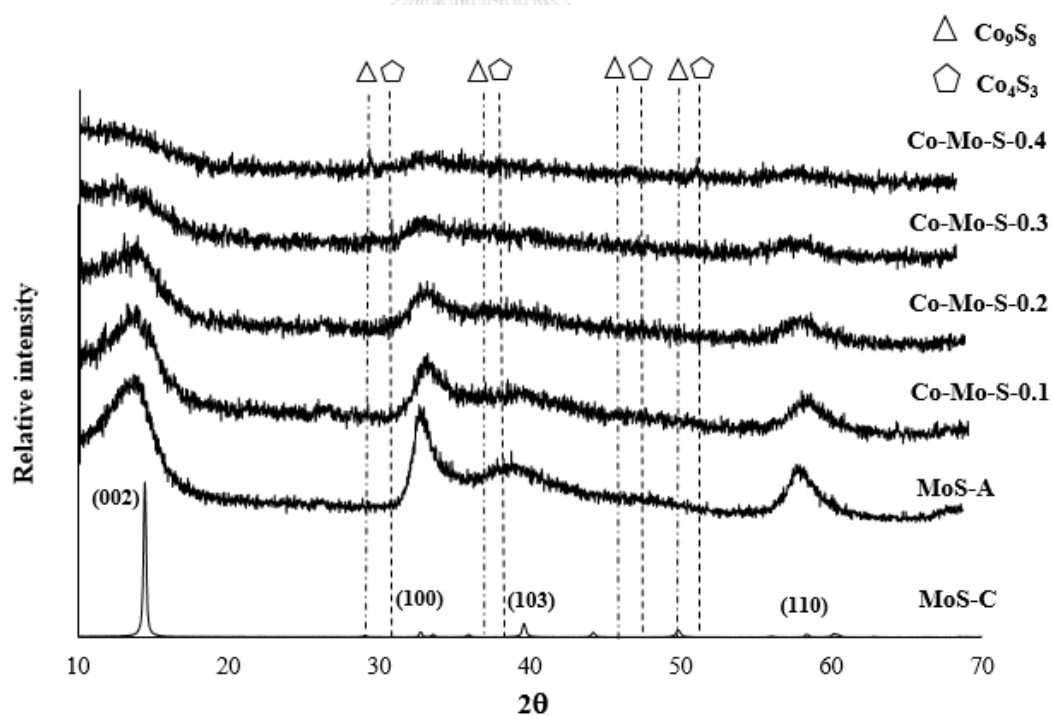


Figure 4.2 XRD pattern of the MoS-C, MoS-A and unsupported Co-Mo sulfide catalysts with various Co/(Mo+Co)

4.1.2 N₂ adsorption-desorption Measurement (BET)

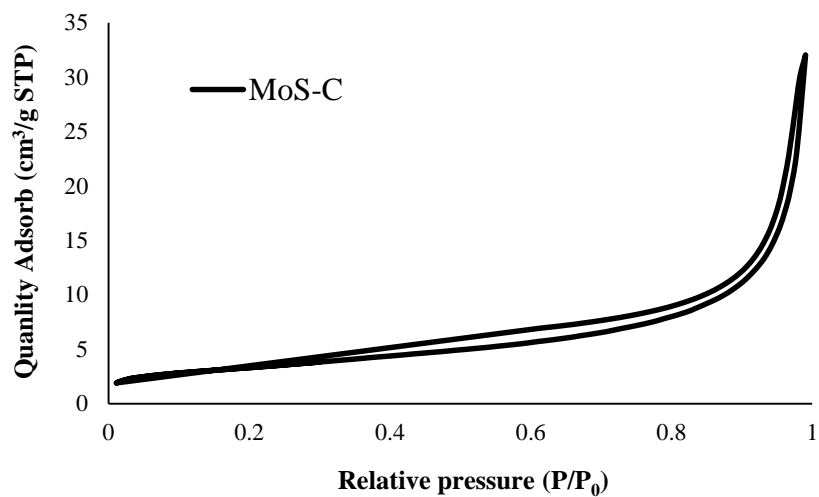
Table 4.1 presents the physical properties of unsupported Mo based sulfide catalysts. The surface area of catalysts was measured before the HDO reaction. The unsupported Mo sulfide catalyst had high surface area (204.32 m²/g) and large pore volume (0.33 cm³/g). After the addition of promoters, a significant decrease in the surface area and pore volume was observed. The addition of promoters (Ni or Co) significantly decreased the surface area and pore volume of unsupported Mo sulfide. These results indicate that the promoter addition influences the surface area of the unsupported Mo sulfide. The variation of surface areas of MoS₂ catalysts could be in the range of few to several hundred square meters per gram depending on the precursor and condition of the synthesis. Alonso et al.[36] and Eijsbouts et al.[37] reported that MoS₂ catalysts prepared from tetraalkylammonium thiomolybdates had surface area in the range of 60-329 and 170-225 m²/g, respectively.

The nitrogen adsorption-desorption isotherms are shown in Figure 4.2 and Figure 4.3 Note, however, that the curves have been shifted along the Y-axis for visualization purposes. All catalysts exhibited type IV isotherms with a hysteresis loop characteristic of mesoporous materials. According to the IUPAC classification, the hysteresis loop of the Mo-S (in the absence of Ni) can be classified as an H1 type, which is usually associated with solids consisting of nearly cylindrical channels or agglomerates or compacts of near uniform spheres [38]. The isotherm results revealed that the addition of Ni into the Mo sulfide changed the pore shape of the catalyst from type H1 to type H3. When only a small amount of Ni was added, the hysteresis loop of the Ni-Mo-S-0.1 showed characteristics between type H1 and type H3, and then with further increased in the amount of promoter the H3 type of hysteresis loop appeared progressively more dominant and narrower (Figure 4.2).

Table 4.1 Composition and properties of the MoS₂-C, MoS₂-A, Ni-Mo-S-A and Co-Mo-S-A unsupported catalysts with various Ni/(Mo+Ni) or Co/(Mo+Co) mole ratios.

Catalysts	Ni/(Mo+Ni) or Co/(Mo+Co)	Surface area (m ² /g)	Pore volume (cm ³ /g)
MoS ₂ -C	0	11.87	0.2
MoS ₂ -A	0	204.32	0.33
Ni-Mo-S-0.1	0.1	116.12	0.18
Ni-Mo-S-0.2	0.2	123.58	0.18
Ni-Mo-S-0.3	0.3	100.49	0.11
Ni-Mo-S-0.4	0.4	46.61	0.07
Co-Mo-S-0.1	0.1	106.02	0.15
Co-Mo-S-0.2	0.2	123.13	0.19
Co-Mo-S-0.3	0.3	31.07	0.05
Co-Mo-S-0.4	0.4	25.89	0.04

(a)



(b)

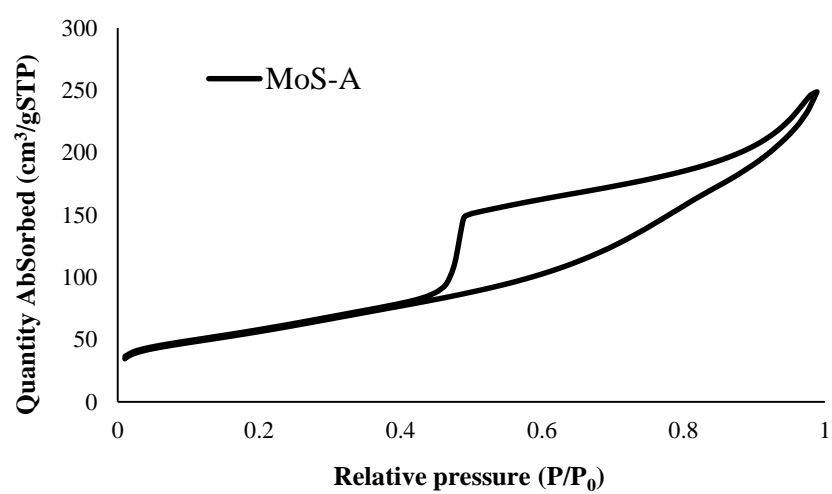


Figure 4.3 N₂ adsorption/desorption isotherms of the (a) MoS-C and (b) MoS-A

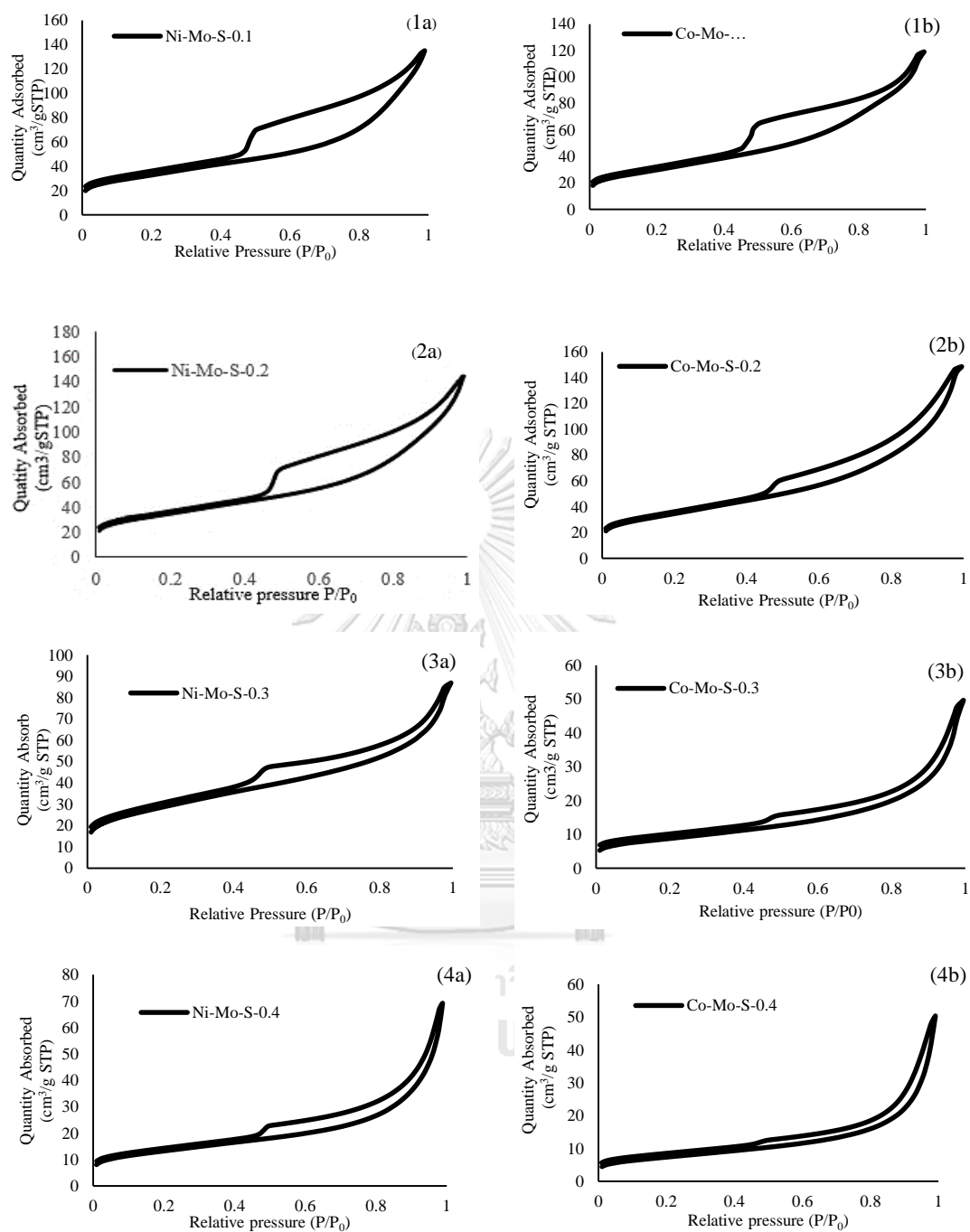


Figure 4.4 N_2 adsorption/desorption isotherms of the (a) Ni–Mo and (b) Co–Mo sulfides of various Ni/(Mo+Ni) or Co/(Mo+Co) mole ratios.

4.1.3 Morphology

Figure 4.4 shows the TEM photographs of unsupported Mo sulfide catalysts with and without Ni or Co promoter (Figure 4.4a and 4.4b). The black thread-like fringes correspond to the MoS₂ slabs and have a spacing of about 0.65 nm that is characteristic of the (0 0 2) basal planes of crystalline MoS₂. Thus, the hydrothermal preparation resulted in long slabs of MoS₂, but with the addition of Ni, these slabs became shorter and more curved, indicating the formation of smaller particles. The decrease of number of layers in the stacks was also observed. The increased in stacking may influence the catalytic performance. For instance, Daage et al. [39] reported that stacking affects the hydrodeoxygenation activity on catalyst. Base on STM observation, rim sites of MoS₂ slabs contain metallic states, which were presumably involved in hydrogenation reaction. Stacking of the MoS₂ decreased the number of exposed rim sites and approaching lower the hydrogenation.

The reduction in the slab length observed by TEM agreed very well with the XRD pattern showing that the smaller sized (0 0 2) basal phase of MoS₂ was generated when Ni or Co promoter was incorporated into the Mo sulfide. The implication is that the growth of MoS₂ crystallized particles was inhibited as Ni or Co promoter was incorporated and this led to smaller crystallized particles compared to the Mo-S.

Table 4.2 Physical properties of the MoS-C, MoS-A, Ni-Mo-S-0.2 and Co-Mo-S-0.2.

Catalysts	Slab length (nm)	Number of stacks	Number of layers
MoS-C	33	1	10
MoS-A	15	8	2-7
Ni-Mo-S-0.2	10	9	5-7
Co-Mo-S-0.2	8	11	2-5

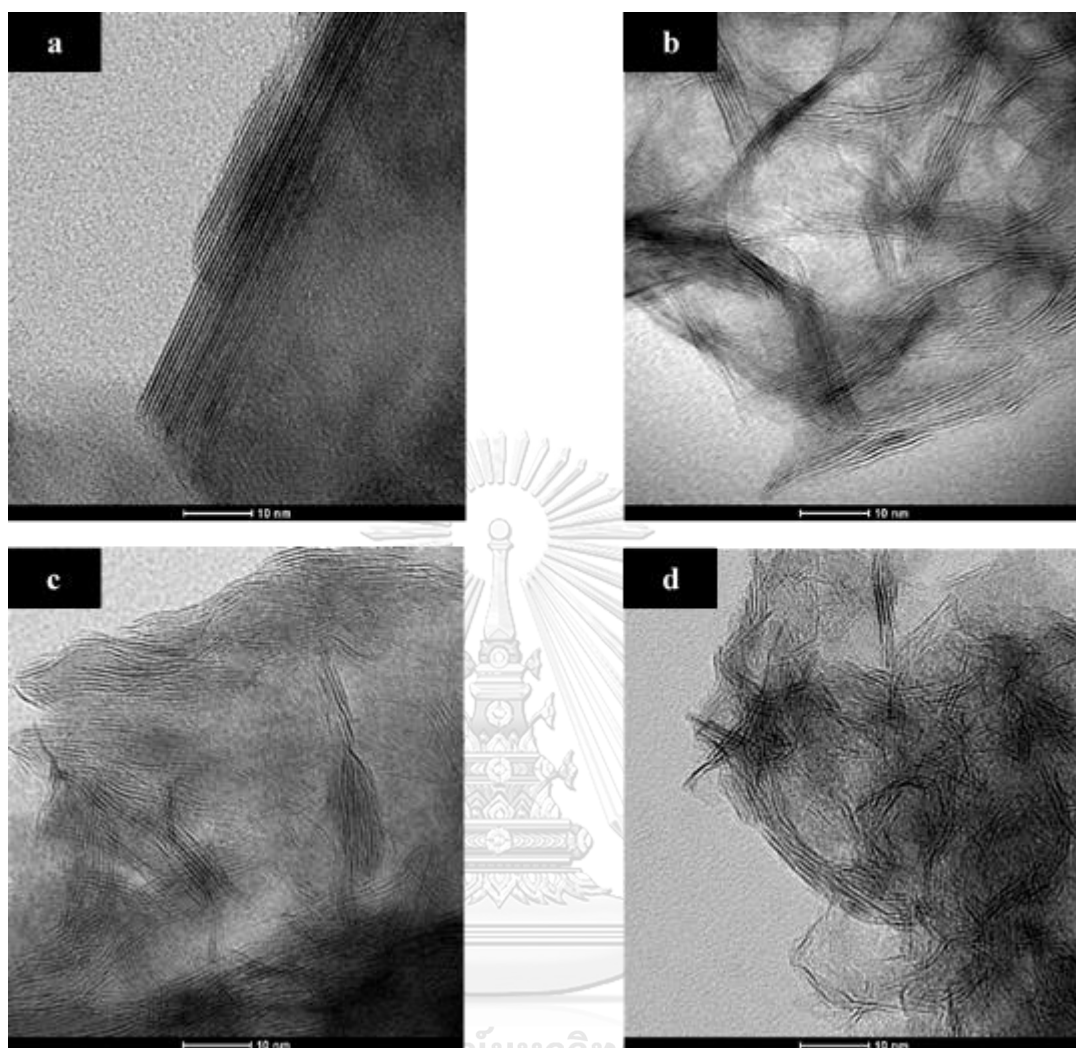


Figure 4.5 TEM images of (a) MoS-C, (b) MoS-A, (c) Ni-Mo-S-0.2 and (d) Co-Mo-S-0.2 catalysts

4.1.4 Temperature-programmed reduction (TPR)

TPR analysis was applied to reveal the presence of various sulfur species whose reactivity is related to their chemical environment. The catalysts showed two reduction zones; a strong peak at low temperatures and a low intensity broad peak in the high temperature zone (Figure 4.5). The low-temperature peak could be assigned to surface sulfur atoms (weakly bonded sulfur) whereas the “bulk reduction” occurred in the higher temperature range. In the low-temperature region, the surface sulfur was reduced and the coordinative unsaturated sites (CUS) were created, which was responsible for the active sites [39]. The TPR analysis also revealed that the position of the peak maxima/minima was affected by the structure and promoter of the MoS₂ catalyst. For the MoS₂-A catalyst, the two main peaks were observed to be centered at 237 and 524 °C, whereas the low temperature zone peak was at a much higher temperature in MoS-C (372 °C), indicating that the reducibility of MoS-A was higher than that of MoS-C. However, the TPR peak in the high temperature region revealed that the reduction temperatures for MoS-A and MoS-C were not significantly different. The addition of Ni or Co promoter caused a major downward shift in the peak position relatively to both high and low temperature TPR peak of MoS-A. It can be concluded that promoter increased the reducibility of MoS-A.

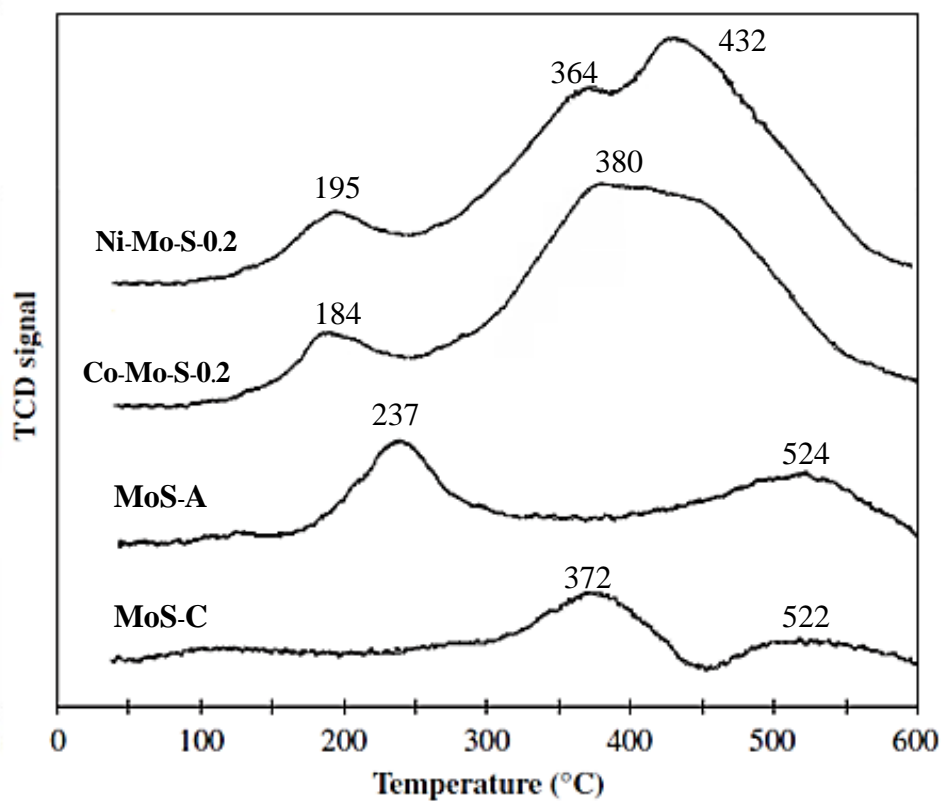


Figure 4.6 TPR profiles of the MoS-C, MoS-A, Ni-Mo-S-0.2 and Co-Mo-S-0.2 catalysts.

4.2 Hydrodeoxygenation of oleic acid

4.2.1 Effect of reaction time

Figure 4.6 and Table 4.3 show the effect of time on hydrodeoxygenation of oleic acid over Ni-Mo-S-0.2 catalyst. The n-C₁₈ yield increased with increasing reaction time and decreased after 8 h, indicating that the increasing reaction time enhanced the hydrodeoxygenation reaction of oleic acid. Accordingly, the optimal condition for hydrodeoxygenation reaction was reaction time of 6 h. The n-C₁₈ yield was 70.3 wt%.

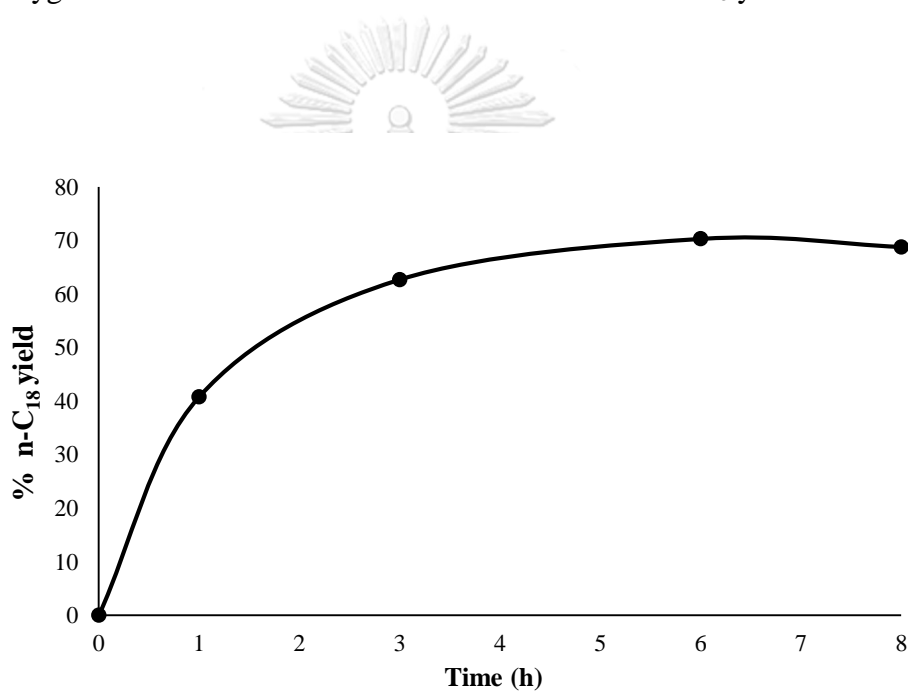


Figure 4.7 Effect of reaction time on n-C₁₈ yield.

Table 4.3 Effect of reaction time on hydrodeoxygenation of oleic acid.

Reaction time (h)	1	3	6	8
Conversion (wt%)	95.1	97.4	100	100
n-alkane content (wt%)	69.0	81.4	89.4	94.0
Selectivity (wt%)				
C ₁₅	2.9	1.7	1.2	1.5
C ₁₆	3.9	1.8	2.0	2.1
C ₁₇	32.9	24.3	18.1	23.2
C ₁₈	60.3	72.2	78.7	73.2
Yield (wt%)				
C ₁₅	2.0	1.4	1.1	1.4
C ₁₆	2.7	1.4	1.8	2.0
C ₁₇	22.7	19.8	16.2	21.8
C ₁₈	41.6	58.8	70.3	68.8

Condition: Temperature = 280 °C, H₂ pressure = 60 bar, oleic acid/catalyst ratio (wt/wt)

= 4, Ni/(Ni+Mo) ratio = 0.2 and catalyst weight = 0.375 wt%

4.2.2 Effects of temperature and pressure

The effects of reaction temperature on the conversion and selectivity of products in the HDO of oleic acid on Ni-Mo-S-0.2 catalyst were studied at constant pressure of 60 bar. The results, as shown in Figure 4.7 and Table 4.4, indicated that the oleic acid conversion significantly increased with increasing temperature and the product distribution also displayed noticeable temperature dependence. The conversion of oleic acid was 87.4 wt% at 250°C, which increased to 100 wt% as temperature increased to 280 °C. The tendency of change in conversion with reaction temperature indicated that the HDO reaction was highly influenced by kinetics. This implied that the temperature was increased the molecule of oleic acid gained more kinetic energy in excess of activation energy to vigorously interact with hydrogen gas at catalyst active sites. The n-C₁₈ selectivity was 69.5 wt% at 250 °C and reached a maximum (78.7 wt%)

at 280 °C and finally decreased to 64.0 wt% at 320 °C. Hensen et al. [40] reported that the analysis of C₁₇ and C₁₈ olefins showed predominantly 1-olefins with some products of isomerization towards more stable internal alkanes. It was suggested that the olefins were predominantly formed via decarbonylation, deoxygenation, hydrocracking and isomerization of long chain olefins. The highest catalyst activity was achieved at temperature of 280 °C corresponding to the high n-C₁₈ yield (70.3 wt%) due to HDO reaction. Whereas increasing temperature (280-320 °C) could enhance the decarboxylation and decarboxylation reactions that the n-C₁₇ selectivity (18.1-31.2 wt%) and n-C₁₇ yield (16.2-28.8 wt%) were also increased.

Figure 4.8 shows the HDO of oleic acid on Ni-Mo-S-0.2 catalyst at different reaction pressure and constant temperature of 280 °C for 6 h. It was observed that the hydrogen pressure had great effect on the conversion and product selectivity. When increasing the hydrogen pressure from 20 bar to 60 bar, the oleic acid conversion increased from 94.2 wt% - 100 wt%. It could be observed that the effect of increasing the initial hydrogen pressure (20-80 bars) is slightly more pronounced on the n-C₁₈ yield (70.3 wt%) than on the n-C₁₇ yield (16.2 wt%). Wang et al [41] reported that increasing hydrogen pressure was favorable for hydrogenation route, which mainly related to the hydrogen solubility. Increasing hydrogen pressure could improve the hydrogen solubility in liquid phase due to hydrogen pressure is function of adsorbed hydrogen on surface of catalyst active sites. In summary, high hydrogen pressure favored hydrodeoxygenation while low hydrogen pressure promoted the decarboxylation and decarboxylation.

Table 4.4 Effects of temperature and pressure on HDO over Ni-Mo-S-0.2 catalyst.

Parameters	Temperature (°C)				Pressure (bar)			
	250	280	300	320	20	40	60	80
Conversion (wt%)	87.4	100	100	100	94.2	95.1	100	100
n-alkane content (wt%)	79.6	89.4	92.5	92.5	80.9	86.3	89.4	84.8
Selectivity (wt%)								
C ₁₅	1.4	1.2	0.9	1.1	1.9	2.5	1.2	2.2
C ₁₆	2.3	2.0	4.2	3.7	5.4	5.3	2.0	3.1
C ₁₇	26.9	18.1	26.0	31.2	32.1	29.3	18.1	22.2
C ₁₈	69.4	78.7	68.9	64.0	60.6	62.9	78.8	72.5
Yield (wt%)								
C ₁₅	1.1	1.1	0.8	1.0	1.5	2.1	1.1	1.9
C ₁₆	1.8	1.8	3.9	3.4	4.4	4.5	1.8	2.6
C ₁₇	21.4	16.2	24.1	28.8	26.0	25.4	16.2	18.8
C ₁₈	55.3	70.3	63.7	59.3	49.0	54.3	70.3	61.5

Condition: Temperature = 280 °C, H₂ pressure = 60 bar, catalyst weight = 0.375 wt%, oleic

acid/catalyst ratio (wt/wt) = 4, and reaction time = 6 h

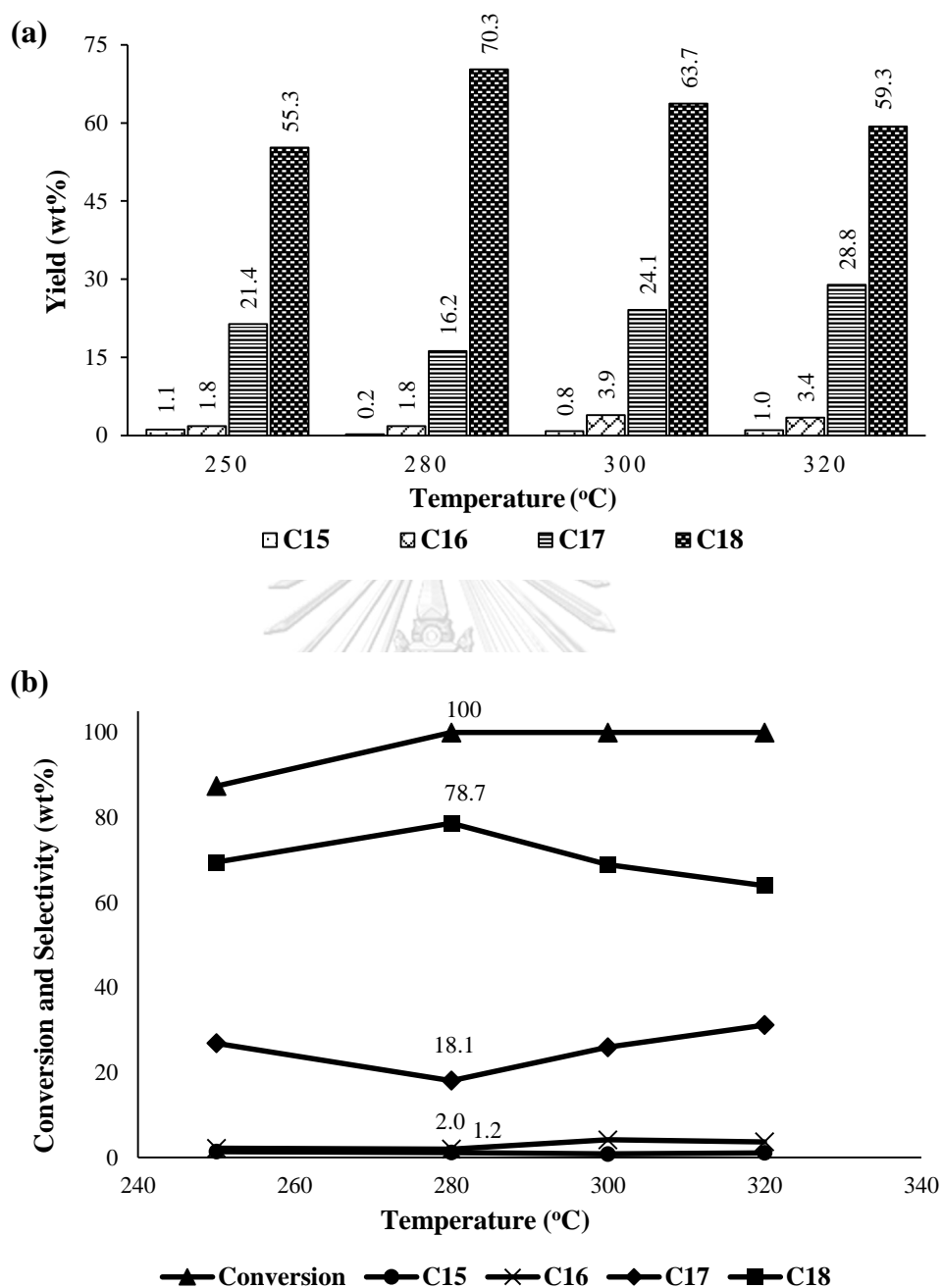


Figure 4.8 Effect of temperature on oleic acid hydrogenation over Ni-Mo-S-0.2 Catalyst, (a) product yield, (b) oleic acid conversion and product selectivity.

Condition: Temperature = 280-320 °C, H₂ pressure = 60 bar, catalyst weight = 0.375 wt%, oleic acid/catalyst ratio (wt/wt) = 4, Ni/(Ni+Mo) = 0.20 and reaction time = 6 h.

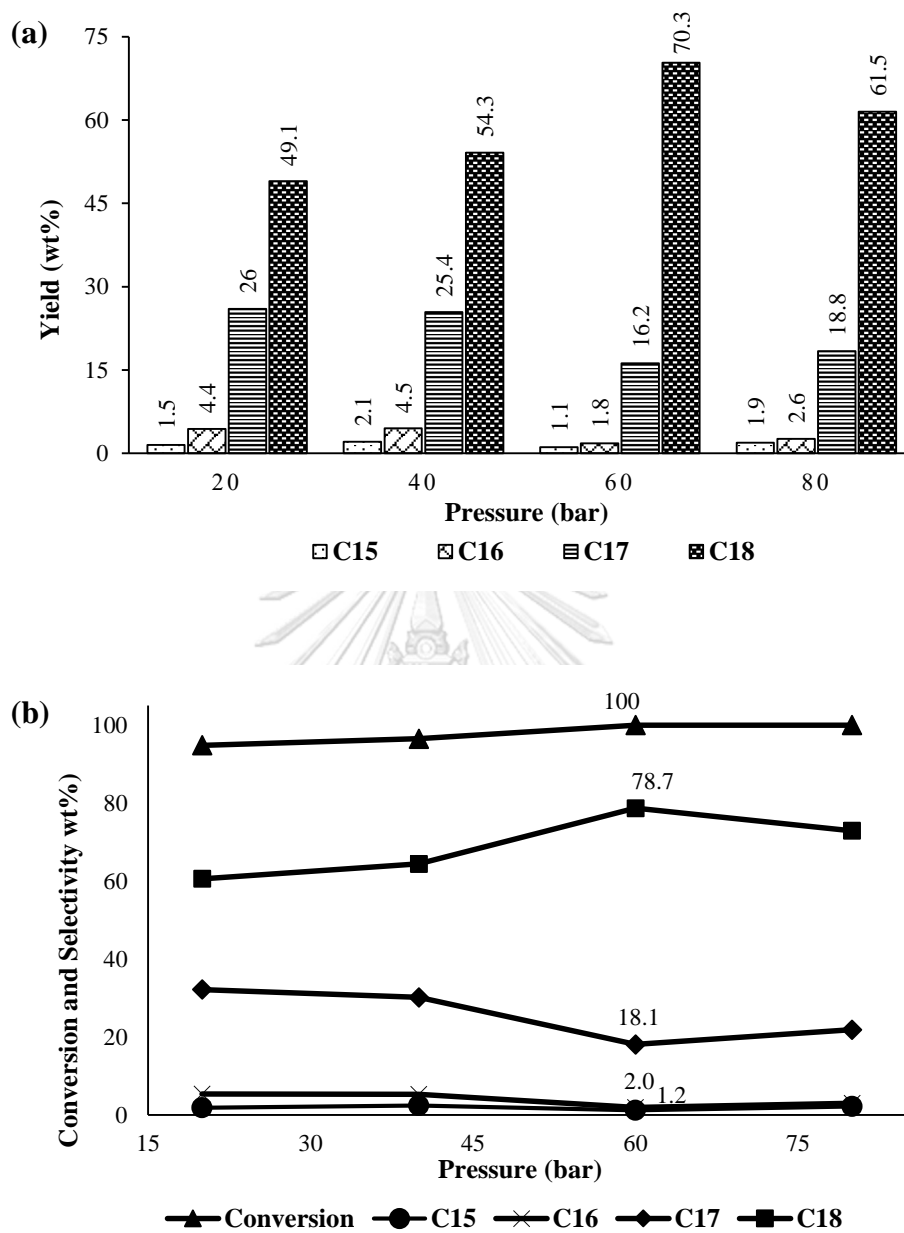


Figure 4.9 Effect of pressure on oleic acid HDO over NiMo sulfide, (a) product yield, (b) oleic acid conversion and product selectivity.

Condition: Temperature = 280 °C, H₂ pressure = 20-80 bar, catalyst weight = 0.375 wt%, oleic acid/catalyst ratio (wt/wt) = 4, Ni/(Ni+Mo) = 0.20 and reaction time = 6 h.

4.2.3 Effects of Ni/(Mo+Ni) and Co/(Mo+Co) mole ratio

The promoting effects are strongly dependent on the amount of Ni or Co added into the amorphous unsupported Mo sulfide is presented in Table 4.5. For addition of Ni promoter at Ni/(Mo + Ni) ratio of 0.1–0.4, the oleic acid conversion gradually increased approaching the value (100 wt%) at Ni/(Mo + Ni) ratio of 0.2. Moreover, the addition at Co promoter of Co/(Mo + Co) ratio of 0.1–0.4, the oleic acid conversion gradually increased approaching the value (96.1wt%) at Co/(Mo + Co) ratio of 0.2. While the activity of the MoS₂ catalyst was improved after the addition of Ni or Co promoter, the surface area showed the opposite trend. This lack of the correlation between the HDO activity and the surface area indicated that the HDO activity of the amorphous Mo sulfide based catalyst was not related to surface area but depended instead on its morphology. The enhanced reaction efficiency was due to the formation of more active catalyst particles with increasing concentration of Ni atoms. However, increasing the Ni/(Mo + Ni) mole ratios above 0.3 or Co/(Mo + Co) mole ratios above 0.3 decreased the obtained conversion efficiency drastically, which is attributed to the formation of a bulk phase of the promoter sulfide that covered part of the active promoted Mo sites.



Table 4.5 Effect of Ni/(Mo+Ni) and Co/(Mo+Co) mole ratio on HDO over unsupported sulfide catalyst

Parameters	Ni/(Ni+Mo)					Co/(Co+Mo)				
	0.1	0.2	0.3	0.4	1	0.1	0.2	0.3	0.4	1
Conversion	95.1	100	97.2	93.8	88.0	87.2	96.1	94.8	91.9	88.4
n-alkane content (wt%)	91.1	89.4	82.8	85.9	12.6	33.5	60.0	34.8	29.1	8.1
Selectivity										
C ₁₅	1.3	1.2	1.8	1.7	0.0	2.9	1.5	5.3	5.2	7.3
C ₁₆	3.0	2.0	0.9	1.1	6.3	3.6	7.5	11.6	4.8	8.6
C ₁₇	20.7	18.1	24.3	28.9	54.6	30.1	21.4	26.4	25.5	65.5
C ₁₈	75.0	78.7	73.0	68.3	39.1	63.4	69.6	56.7	64.5	18.6
Yield(wt%)										
C ₁₅	1.2	1.1	1.5	1.5	0.0	1.0	0.9	1.9	1.5	0.6
C ₁₆	2.7	1.8	0.8	1.0	0.8	1.2	4.5	4.0	1.4	0.7
C ₁₇	18.9	16.2	20.0	24.8	6.9	10.1	12.8	9.2	7.2	5.3
C ₁₈	68.3	70.3	60.1	58.6	4.9	21.2	41.8	19.7	18.8	1.5

Condition : Temperature = 280 °C, H₂ pressure = 60 bar, catalyst weight 0.075 wt%, oleic acid/catalyst (wt/wt) = 4, and reaction time = 6 h

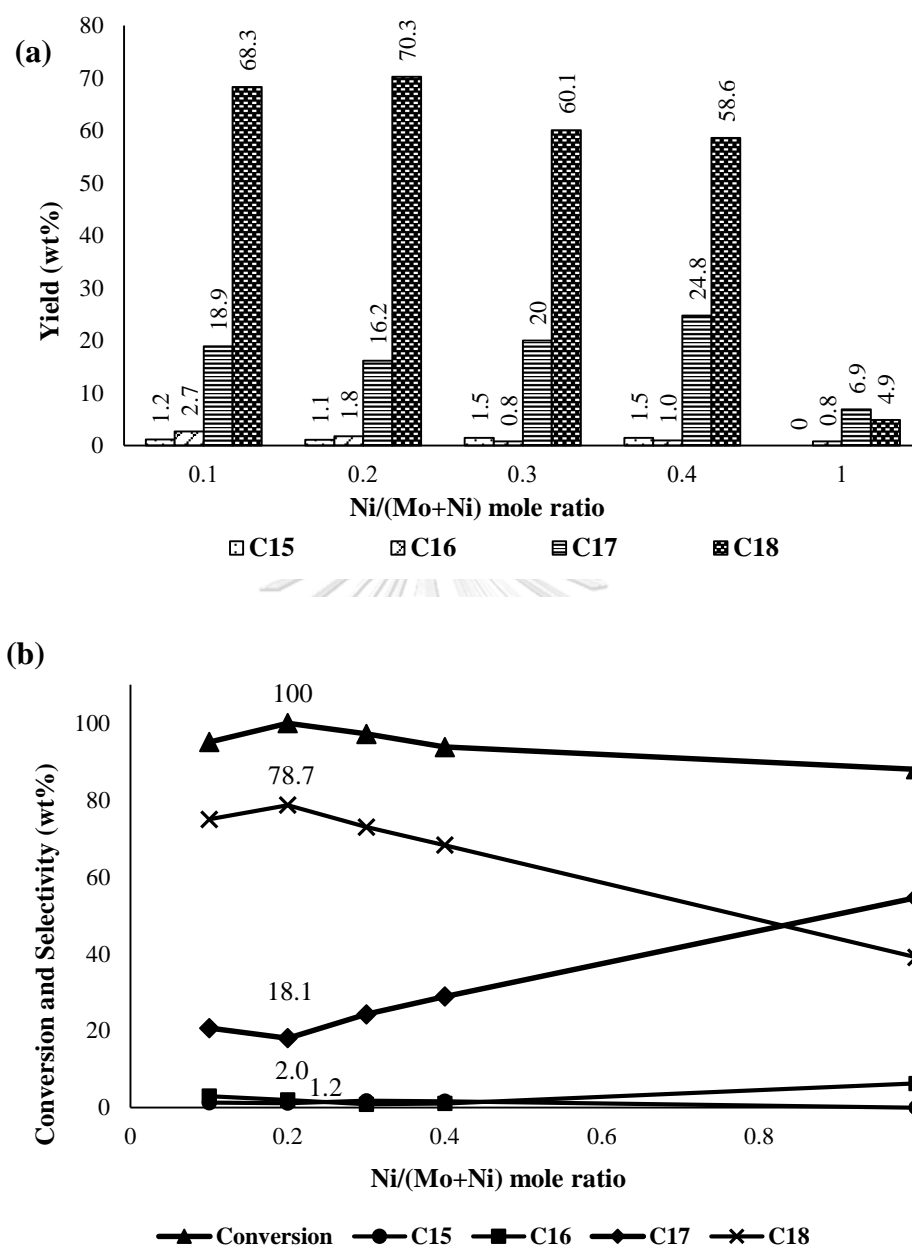


Figure 4.10 Effect of Ni/(Mo+Ni) mole ratio on product selectivity over NiMo sulfide,

(a) product yield, (b) oleic acid conversion and product selectivity.

Condition: Temperature = 280 °C, H₂ pressure = 60 bar, Ni/(Ni+Mo) = 0.2, catalyst weight = 0.375 wt%, oleic acid/catalyst ratio (wt/wt) = 4, and reaction time = 6 h.

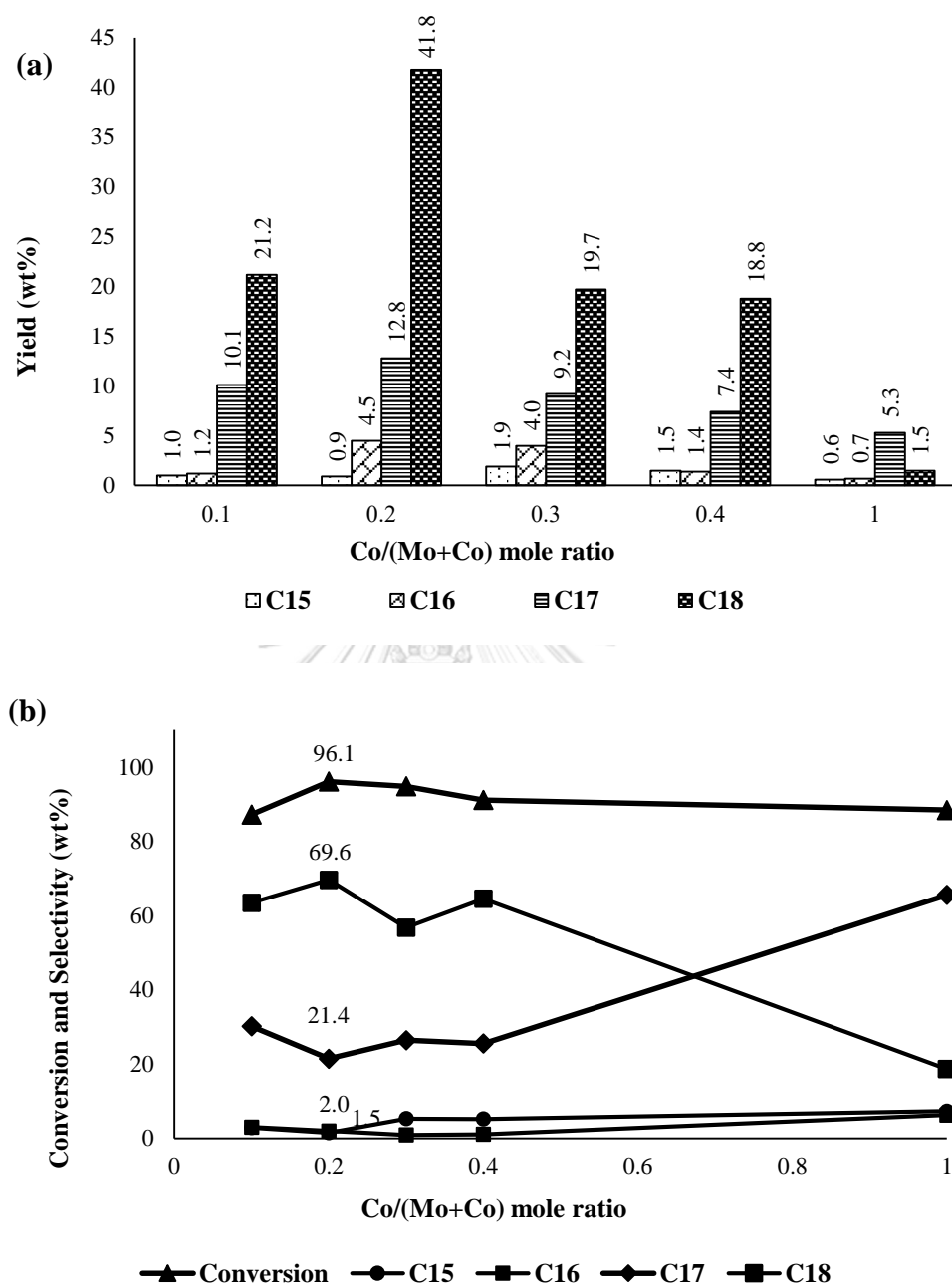


Figure 4.11 Effect of Co/(Mo+Co) mole ratio on product selectivity over CoMo sulfide, (a) product yield, (b) oleic acid conversion and product selectivity.

Condition : Temperature = 280 °C, H₂ pressure = 60 bar, Ni/(Ni+Mo) = 0.2, catalyst weight = 0.375 wt%, oleic acid/catalyst ratio (wt/wt) = 4, and reaction time = 6 h.

4.2.4 Effect of oleic acid to catalyst ratio

Figure 4.11 shows oleic conversion and product yield obtained for different oleic acid/catalyst ratio at constant pressure of 60 bar and temperature of 280 °C. For increasing oleic acid amount at oleic acid/catalyst ratio of 1.3–4 (wt/wt), the oleic acid conversion gradually increased approaching the value (100 wt%) at oleic acid/catalyst ratio of 4. At above oleic acid/catalyst ratio of 8, the conversion decreased due to decreasing catalyst amount. It could be observed that the effect of increasing oleic acid/catalyst ratio (1.4-8 (wt/wt)) is slightly more pronounced on the n-C₁₈ yield (70.3 wt%) than on the n-C₁₇ yield (16.2 wt%). Therefore, oleic acid/catalyst ratio of 4 was favorable for HDO pathway and higher n-C₁₈ yield. The oleic acid/catalyst ratio above 8 could increase the decarbonylation and decarboxylation pathway.

Table 4.6 Effect of oleic acid/catalyst ratio on HDO over unsupported sulfide catalyst

Oleic acid/catalyst ratio (wt/wt)	1.3	4	8	12
Conversion (wt%)	100	100	96.4	96.1
n-alkane content (wt%)	87.8	89.4	78.9	83.2
Selectivity (wt%)				
C ₁₅	1.3	1.2	0.9	0.7
C ₁₆	2.5	2.0	2.1	2.2
C ₁₇	23.6	18.1	20.7	25.3
C ₁₈	72.6	78.7	76.3	71.8
Yield (wt%)				
C ₁₅	1.1	1.1	0.7	0.6
C ₁₆	2.2	1.8	1.7	2.2
C ₁₇	20.8	16.2	16.3	21.0
C ₁₈	63.7	70.3	60.0	59.4

Condition: Temperature = 280 °C, H₂ pressure = 60 bar, catalyst weight = 0.375 wt%, and reaction time = 6 h

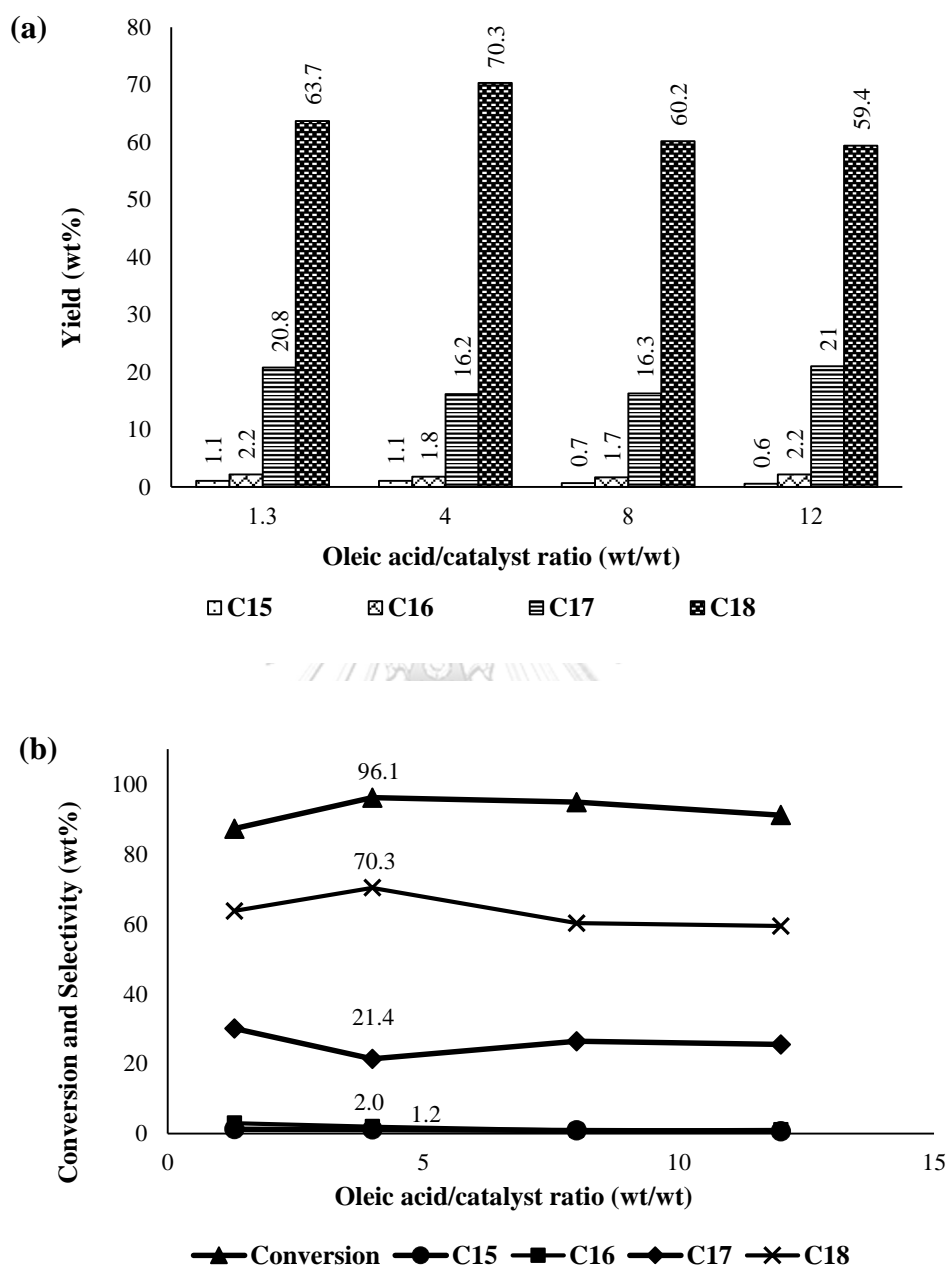


Figure 4.12 Effect of oleic acid/ catalyst ratio on product selectivity over NiMo sulfide, (a) product yield, (b) oleic acid conversion and product selectivity.

Condition: Temperature = 280 °C, H₂ pressure = 60 bar, catalyst weight = 0.375 wt%, oleic acid/catalyst ratio (wt/wt) = 4, and reaction time = 6 h.

4.2.5 Comparison of sulfide catalysts on oleic acid HDO

Comparison of the crystalline and amorphous MoS₂ catalysts activity, product selectivity and product yield, based on oleic acid conversion by hydrogenation, are presented in Table 4.7. Regarding sulfide catalysts, it has been proposed that carboxylic acid compounds react through three pathways involving direct C=O bonds scission (direct hydrodeoxygenation, HDO) yielding n- C₁₈ products and the other via decarboxylation and decarbonylation leading to yielding n-C₁₇ products.

As shown in Table 4.4, the oleic acid HDO conversion obtained from hydrogenation using the Ni-Mo-S-0.2 catalyst (100 wt%) was almost higher than without catalyst (78.9 wt%), MoS-C (84.6 wt%), MoS-A (91.9 wt%) and Co-Mo-S-0.2 (96.1wt%). The activity of the catalysts decreased in the order Ni-Mo-S-0.2 > Co-Mo-S-0.2 > MoS-A > MoS-C > without catalyst. The hydrogenation of oleic acid on MoS-A catalyst was greatly enhanced by promoter addition and this high catalytic activity was essentially due to the increase in rate of HDO reaction (Figure 4.13).

Table 4.7 Comparison of sulfide catalysts on oleic acid HDO

Catalysts	Without catalyst	MoS-C	MoS-A	Ni-Mo-S-0.2	Co-Mo-S-0.2
Conversion(%)	78.9	84.6	91.9	100	96.1
n-alkane content (%)	5.6	57.0	59.9	89.4	60.0
Selectivity(%)					
C ₁₅	0	0.0	0.8	1.2	1.5
C ₁₆	0	9.1	7.2	2.0	7.5
C ₁₇	51.7	27.6	24.8	18.1	21.4
C ₁₈	48.3	63.3	67.2	78.7	69.6
Yield (%)					
C ₁₅	0	0.0	0.5	1.1	0.9
C ₁₆	0	5.2	4.3	1.8	4.5
C ₁₇	2.9	15.7	14.9	16.2	12.8
C ₁₈	2.7	36.1	40.2	70.3	41.8

Condition: Temperature = 280 °C, H₂ pressure = 60 bar, catalyst weight = 0.375 wt%,

oleic acid/catalyst = 4, and reaction time = 6 h

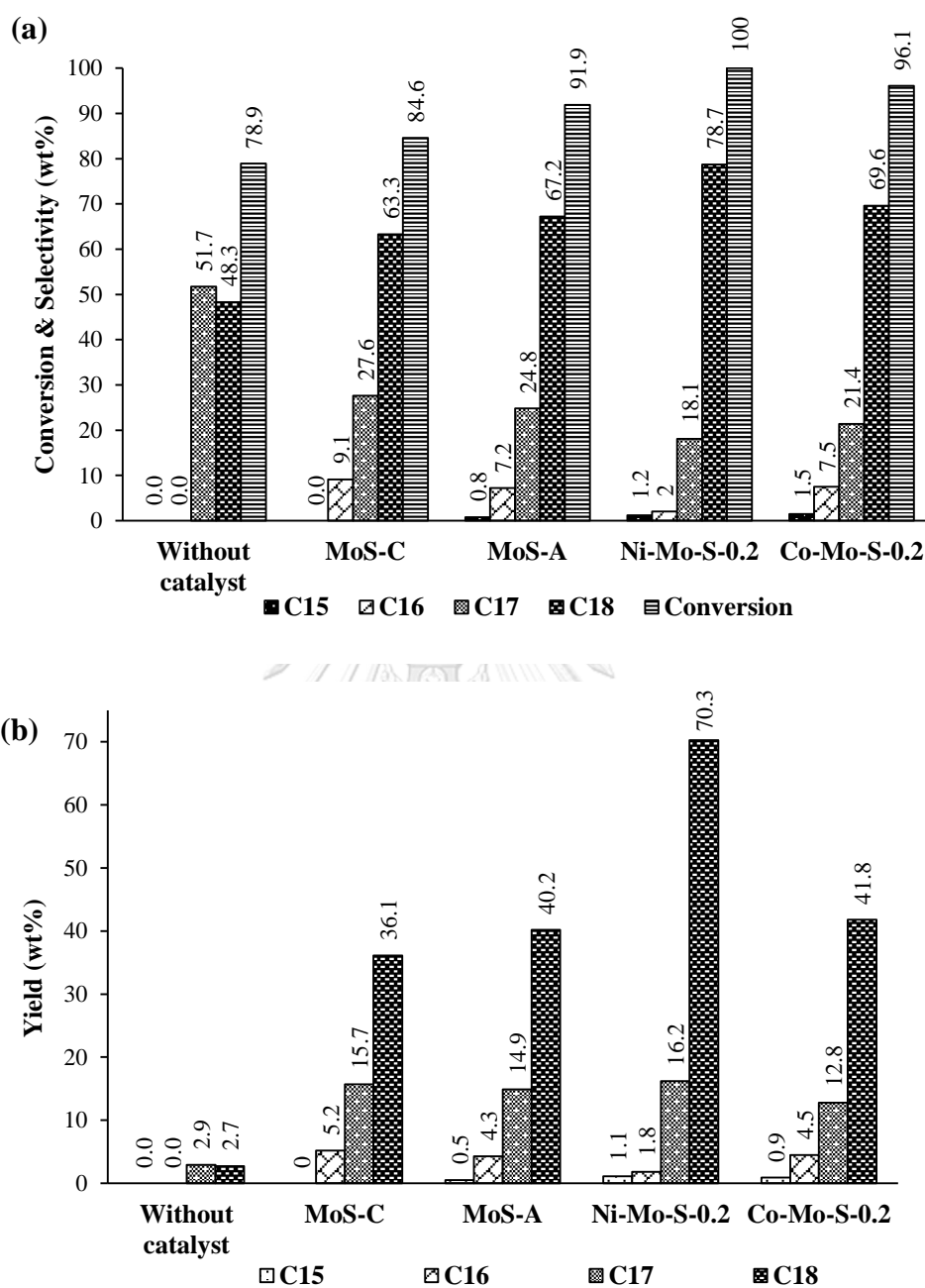


Figure 4.13 Comparison of sulfide catalysts on oleic acid HDO, (a) oleic acid conversion and product selectivity, (b) product yield.

Condition: Temperature = 280 °C, H₂ pressure = 60 bar, catalyst weight = 0.375 wt%, oleic acid/catalyst = 4, and reaction time = 6 h

4.2.6 Oxygen contents of products and oxygen removal efficiency

The HDO of oleic acid is confirmed by CHON analysis of the products. Table 4.8 presents oxygen content (wt%) and oxygen removal efficiency (wt%) of liquid products from HDO of oleic acid over MoS₂-C, MoS₂-A, Ni-Mo-S-0.2 and Co-Mo-S-0.2 catalysts. These results showed that unsupported Ni-Mo-S-0.2 catalysts gave the highest oxygen removal efficiency (66.7 wt%) in oleic acid and highest oxygen removal efficiency (59.1 wt%) in palm oil.

Table 4.8 Oxygen contents of products and oxygen removal efficiency

Reactant	Catalysts	O (wt%)	Oxygen removal efficiency (wt%)
Oleic acid	-	11.4	-
Oleic acid	MoS-C	10.2	10.5
Oleic acid	MoS-A	9.2	19.3
Oleic acid	Ni-Mo-S-0.2	3.8	66.7
Oleic acid	Co-Mo-S-0.2	5.3	53.5
Palm oil	-	12.2	-
Palm oil	Ni-Mo-S-0.2	5.0	59.0
Palm oil	Co-Mo-S-0.2	6.7	45.1

Condition: Temperature = 280 °C, H₂ pressure = 60 bar, catalyst weight = 0.375 wt%,

oleic acid/catalyst ratio = 4, and Reaction time = 6 h

CHAPTER 5

CONCLUSIONS

5.1 Conclusions

The study of unsupported sulfide catalysts is a promising route for development of efficient hydrotreating catalysts. Hydrothermal preparation of transition-metal sulfides catalysts is particularly interesting because this method provides a highly active catalysts which does not require the sulfidation step. The unsupported Ni-Mo and Co-Mo sulfide catalysts prepared by hydrothermal method have excellent catalytic activity of HDO performance. Unsupported Mo sulfide catalyst showed high surface area without using any promoters. The addition of promoters (Ni or Co) resulted in significant decrease in surface area and pore volume of unsupported Mo sulfide. However, on the basis of TEM and XRD analysis, the addition of promoters led to the increase in curvature of MoS₂ slabs and the decrease in slab length. This is probably because Ni or Co may be located on edge of MoS₂ structure and prevents the growth (or aggregation) of crystalline. A part of the added Co and Ni promoters may be present as Co sulfide and Ni sulfide, as also suggested by XRD. This high activity was supported by TPR analysis showing that the addition of promoter to the unsupported Mo sulfide causes a significant downward shift of the first peak reduction temperature which suggests the decrease in the metal sulfur bond energy.

The HDO of oleic acid on unsupported Co-Mo and Ni-Mo sulfide was greatly enhanced by promoter addition. High pressure favored HDO pathway, while high temperature strongly affected the decarboxylation and decarbonylation pathways. At optimal condition as temperature of 280°C, reaction times of 6 h and hydrogen pressure of 60 bar, the Ni-Mo sulfide catalysts with Ni/(Ni+Mo) ratio of 0.2 had shown better performance for the oleic acid HDO than Co-Mo sulfide in term of oleic acid conversion (100 wt%), n-C₁₈ selectivity (78.8 wt%) and n-C₁₈ yield (70.3 wt%).

5.2 Suggestions of the Future Work

1. Study the hydrodeoxygenation performance of other unsupported bimetallic sulfide catalysts using oleic acid as model of palm oil.
2. Study the effects of operating parameters on the activity and selectivity of unsupported Co-Mo and Ni-Mo sulfide catalysts for the hydrodeoxygenation of palm oil



REFERENCES



จุฬาลงกรณ์มหาวิทยาลัย
CHULALONGKORN UNIVERSITY

REFERENCES

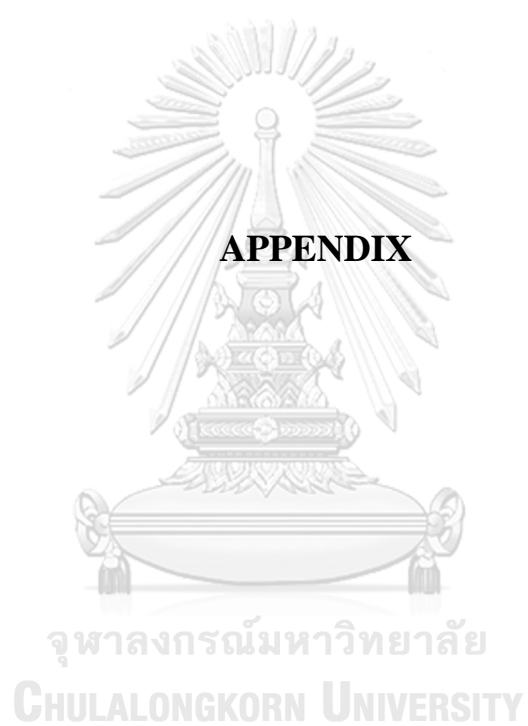
- [1] Zhang, Q., Chang, J., Wang, T., and Xu, Y. Review of biomass pyrolysis oil properties and upgrading research. *Energy Conversion and Management* 48 (2007): 87-92.
- [2] Mullen, C.A. and Boateng, A.A. Chemical Composition of Bio-oils Produced by Fast Pyrolysis of Two Energy Crops. *Energy Fuels* 22 (2008): 2104-2109.
- [3] Mohan, D., Pittman, C.U., Jr., and Steele, P.H. Pyrolysis of Wood/Biomass for Bio-oil: A Critical Review. *Energy Fuels* 20 (2006): 848-889.
- [4] Demirbas A., Biomass resource facilities and biomass conversion processing for fuels and chemicals. *Energy Conversion Management* 42 (2001) :1357-1378.
- [5] Shuit S.H., Tan K.T., Lee K.T. and Kamaruddin A.H. Oil palm biomass as a sustainable energy source: a Malaysian case study. *Energy* 34 (2009):1225–1235.
- [6] Bicalho T, Bessou C and Pacca SA. Land use change within EU sustainability criteria for biofuels: the case of oil palm expansion in the Brazilian Amazon. *Renew Energy* 89 (2016): 588–597.
- [7] Czernik S. and Bridgwater A.V. Overview of applications of biomass fast pyrolysis oil. *Energy & Fuels* 18 (2004): 590-598.
- [8] Guzman A., J.E.T., Prada P. and Nunez M. Hydroprocessing of crude palm oil at pilot plant scale. *Catalysis Today* 156 (2010): 38-43.
- [9] Chianelli R. R. Fundamental- studies of transition- metal sulfide hydrodesulfurization catalysts. *Catalysis Reviews Science and Engineering* 26 (1984): 361-393.

- [10] Ratnasamy P. and Sivasanker S. Structural chemistry of Co- Mo- alumina catalysts. *Catalysis Reviews-Science and Engineering* 22 (1980): 401-429.
- [11] Peng B., Zhao C., Kasakov S., Foraita S. and Lercher J.A. Manipulating catalytic pathways: deoxygenation of palmitic acid on multifunctional catalysts. *Chemistry* 19 (2013): 4732–4741.
- [12] Hilton M.R. and Fleischauer P.D. TEM lattice imaging of the nanostructure of early-growth sputter-deposited MoS₂ solid lubricant films. *Journal of Materials Research* 5 (1990): 406-421.
- [13] Voorhoev R.J. and Stuijver J.C.M. Mechanism of hydrogenation of cyclohexene and benzene on nickel-tungsten sulfide catalysts. *Journal of Catalysis* 23 (1971): 243-252.
- [14] Farragher A.L. and Cossee P. Catalytic chemistry of molybdenum and tungsten sulfides and related ternary compounds. *Proceeding of the Fifth International Congress on Catalysis* 2 (1973): 1301-1318.
- [15] Inamura K. and Prins R. Co-Mo sulfides in the hydrodesulfurization of thiophene. *Journal of Catalysis* 147 (1994): 515-524.
- [16] Schweiger H., Raybaud P., Krause G. and Toulhoat H. Shape and edged sites modifications of MoS₂ catalytic nanoparticle induced by working condition: theoretical study. *Journal of Catalysis* 207 (2002): 76-87.
- [17] Whitehurst D.D., Isoda T. and Mochida I. Present state of the art and future challenges in the hydrodesulfurization of polyaromatic sulfur compounds. *Advances in Catalysis* 42 (1998): 345-471.
- [18] Schuit G. C. A. and Gates B. C. Chemistry and engineering of catalytic hydrodesulfurization. *AICHE Journal* 19 (1973): 417-438 1973.

- [19] Voorhoev R.J and Stuver J. C.M. Kinetics of hydrogenation on supported and bulk nickel-tungsten sulfide catalysts. *Journal of Catalysis* 23 (1971): 228-235.
- [20] Yoneyama Y. and Song C. S. A new method for preparing highly active unsupported Mo sulfide. Catalytic activity for hydrogenolysis of 4(1-naphthylmethyl) bibenzyl. *Catalysis Today* 50 (1999): 19–27.
- [21] Yang Y., Zhang X. and Wang L. Hydrotreating of C18 fatty acids to hydrocarbons on sulphided NiW/SiO₂–Al₂O₃. *Fuel Processing Technology* 116 (2013): 165–174.
- [22] Olivas A., Zepeda T.A., Villalpando I. and Fuentes S. Performance of unsupported Ni(Co,Fe)/MoS₂ catalysts in hydrotreating reactions. *Catalysis Communications* 9 (2008): 1317-1328.
- [23] Devers E., Afanasiev P., Jouguet B. and Vrinat M. Hydrothermal syntheses and catalytic properties of dispersed molybdenum sulfides. *Catalysis Letters* 82 (1-2) (2002): 13-17.
- [24] Yang Y.Q., Tye C.T. and Smith K.J. Influence of MoS₂ catalyst morphology on the hydrodeoxygenation of phenols. *Catalyst Communications* 9 (2008): 1364-1368.
- [25] Yoosuk B., Kim J.H., Song C.S., Ngamcharussrivichai C. and Prasassarakich P. High active MoS₂, CoMoS₂ and NiMoS₂ unsupported catalysts prepared by hydrothermal synthesis for hydrodesulfurization of 4,6-dimethyldibenzothiophene. *Catalyst Today* 130 (2008): 14-23.
- [26] Yoosuk B., Tumnanthong D. and Prasassarakich P. Unsupported MoS₂ and CoMoS₂ catalysts for hydrodeoxygenation of phenol. *Chemical Engineering Science* 79 (2012): 1-7.

- [27] Srifa A. , Faungnawakij K. , Itthibenchapong V. , Viriya-empikul N. , Charinpanitkul T., Assabumrungrat S. Production of bio-hydrotreating diesel by catalytic hydrotreating of palm oil over NiMoS₂/ Al₂O₃ catalyst. *Bioresource Technology* 158 (2014): 81-91.
- [28] Kiatkittipong W. , Phimsen S. , Kiatkittipong K. , Wongsakulphasath S. and Laosiripoja N. Diesel-like hydrocarbon production from hydroprocessing of relevant refining palm oil. *Fuel Processing Technology* 116 (2013): 16-26.
- [29] Toba M. , Abe Y. and Yosimura Y. Hydrodeoxygenation of waste vegetable oil over sulfide catalysts. *Catalysis Today* 164 (2010): 533-537.
- [30] Ayodele O.B., Togunwa O.S. and Abbas H.F. Preparation and characterization of alumina supported nickel-oxalate catalyst for hydrodeoxygenation of oleic acid into normal and iso-octadecane biofuel. *Energy Conversion and Management* 88 (2014): 1104-1110.
- [31] Shim J.O., Jeong D.W., Jang W.J., Jeon K.W., Kim S.H., Jeon B.H., Roh H.S., Na J.G. , Oh Y. K. , Han S. S. and Ko C. H. Optimization of unsupported CoMo catalyst for decarboxylation of oleic acid. *Catalysis Communications* 67 (2015): 16-20.
- [32] Nikulshin P.A., Salnikov V.A., Varakin A.N. and Kogan V.M. The use of CoMoS catalysts supported on carbon-coated alumina for hydrodeoxygenation of guaiacol and oleic acid. *Catalysis Today* 271 (2016): 45-55.
- [33] Kubicka D. and Kaluza L. Deoxygenation of vegetable oils over sulfided Ni, Mo and NiMo catalysts. *Applied Catalysis A: General* 372 (2010): 199-208.
- [34] Miao C., Marin-Flores O., Davidson S., Li T., Dong T., Gao D., Wang Y., Garcia-Perez M. and Chen S. Hydrothermal catalytic deoxygenation of palmitic acid over nickel catalyst. *Fuel* 166 (2016): 302-308.

- [35] Yoosuk B., Tumnanthong D. and Prasassarakich P. Amorphous unsupported Ni-Mo sulfide prepared by one step hydrothermal method for phenol hydrodeoxygenation. *Fuel* 91 (2012): 246-252.
- [36] Alonso G., Berhault G., Aguilar A., Collins V., Ornelas C. and Fuentes S.R.R. Characterization and HDS activity of mesoporous MoS₂ catalysts prepared by In situ activation of tetraalkylammonium thiomolybdates Chianelli. *Journal of Catalysis* 208 (2002): 359–369.
- [37] Eijsbouts S., Mayo S.W. and Fujita K. Unsupported transition metal sulfide catalysts: from fundamentals to industrial application. *Applied Catalysis A : General* 322 (2007): 56-66.
- [38] Horacek J., Tisler Z., Rubas V. and Kubicka D. HDO catalysts for triglycerides conversion into pyrolysis and isomerization feedstock. *Fuel* 121 (2013): 57–64.
- [39] Daage M. and Chianelli R.R. Structure-function relations in molybdenum sulfide catalysts - the rim-edge model. *Journal of Catalysis* 149 (1994): 414-427.
- [40] Hensen E.J.M. and Couman A.E. A model compound (methyl oleate, oleic acid, triolein) study of triglyceride hydrodeoxygenation over alumina-supported Ni-Mo sulfide. *Applied Catalysis B : Environmental* 201 (2016): 290-301.
- [41] Wang W., Li L., Wu K., Zhang K. and Yang Y. Preparation of Ni-Mo-S catalysts by hydrothermal method and their hydrodeoxygenation properties. *Applied Catalysis A : General* 495 (2015): 8-16.



Appendix A

GC-MS parameter for liquid product analysis

GC-MS analysis was performed on an Agilent 7000C GC/MS Triple Quad with HP-INNOWAX column (30 m x 0.25 mm x 0.25 μ m). 0.2 μ L of liquid sample was injected into GC with split ratio of 20. The injection and detector temperatures were 225 $^{\circ}$ C. The temperature program was increased from 60 $^{\circ}$ C to 250 $^{\circ}$ C at a rate of 10 $^{\circ}$ C/min for 5 min and maintained at 250 $^{\circ}$ C for 15 min. Liquid products were identified either by comparison with retention times of reference compounds and with help their MS fragmentation pattern using the National Institute and Technology NIST02 library database software. MS data and chromatograms were recorded using the Chemstation software. The results are shown in Figure A-1.

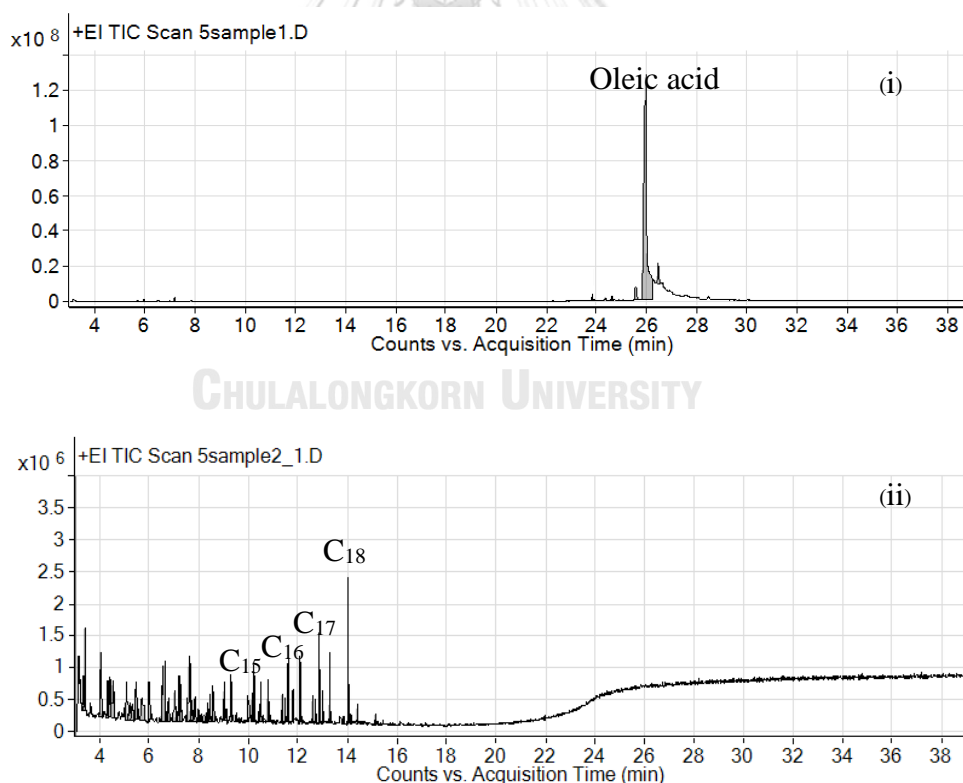
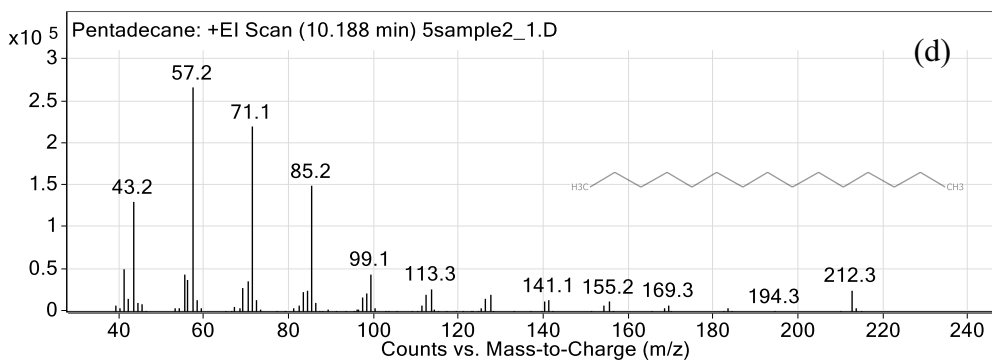
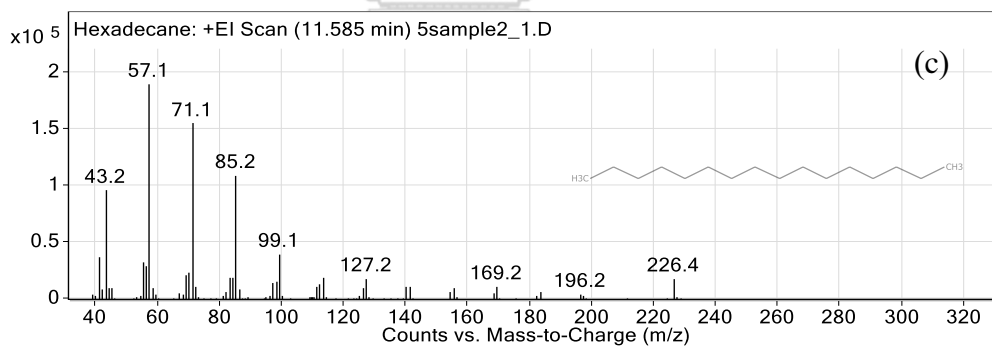
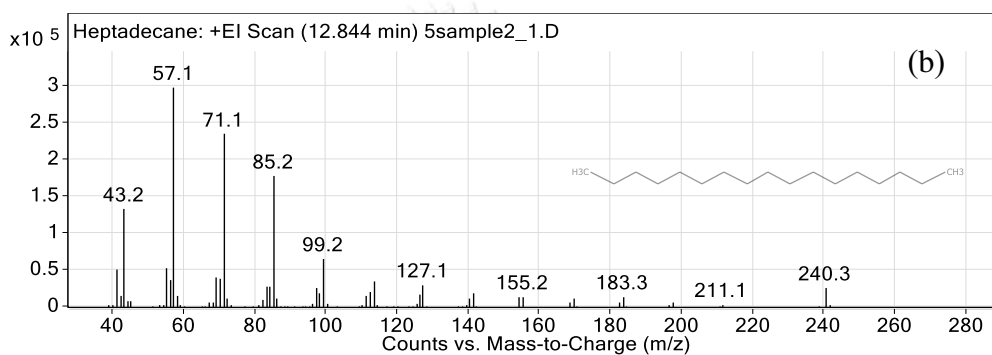
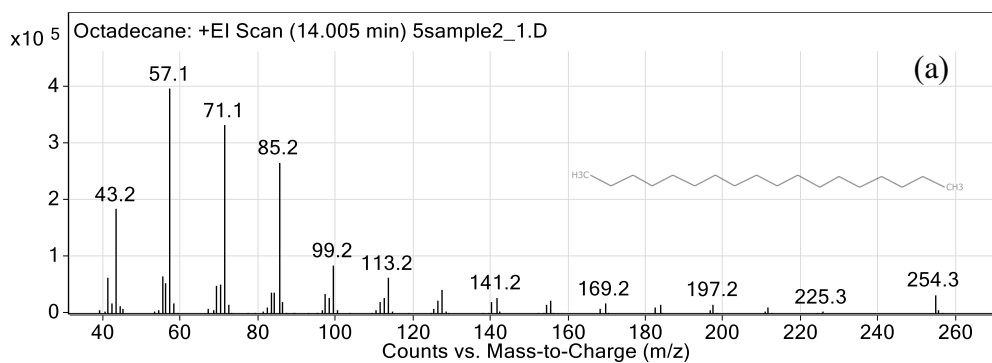
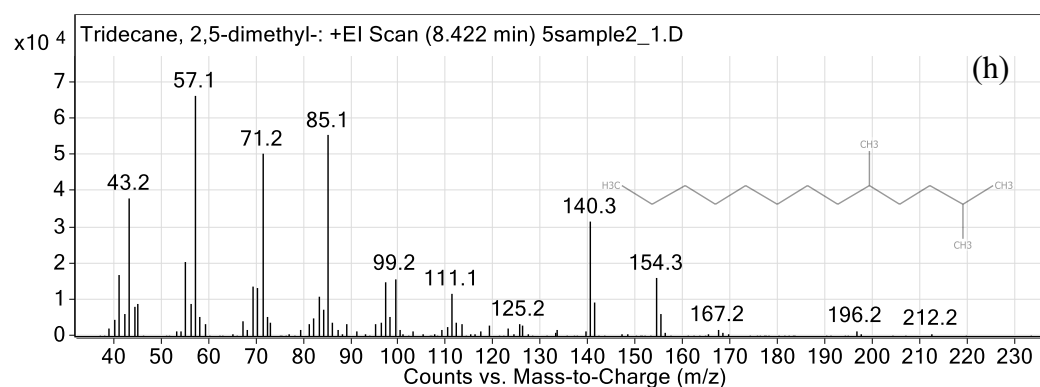
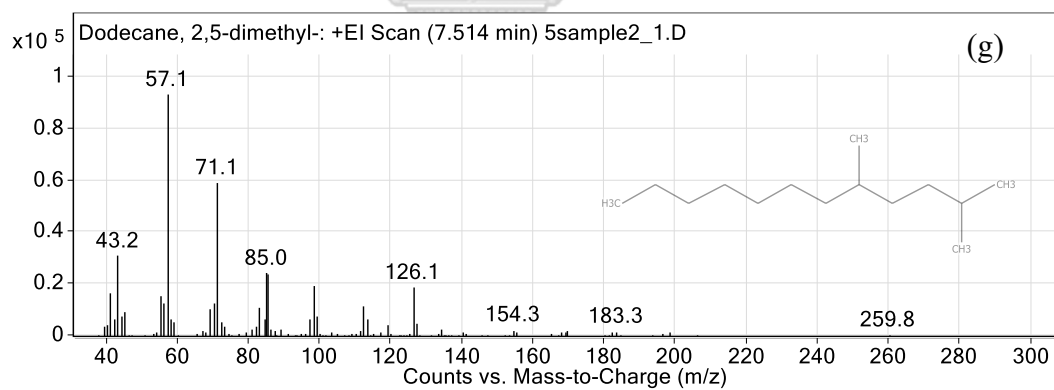
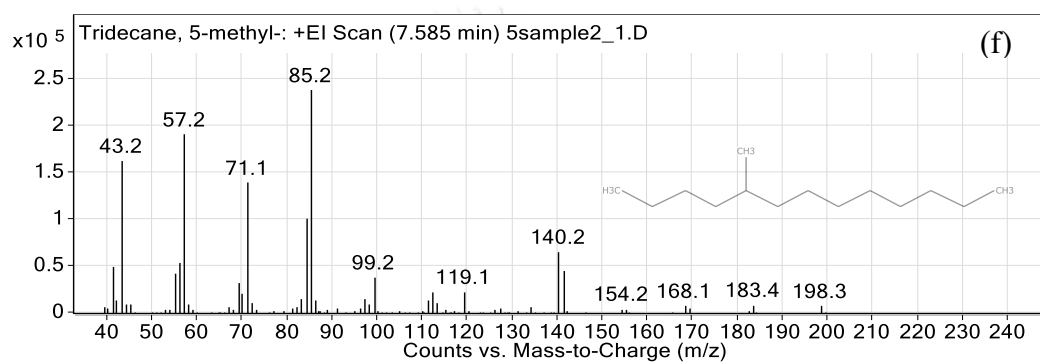
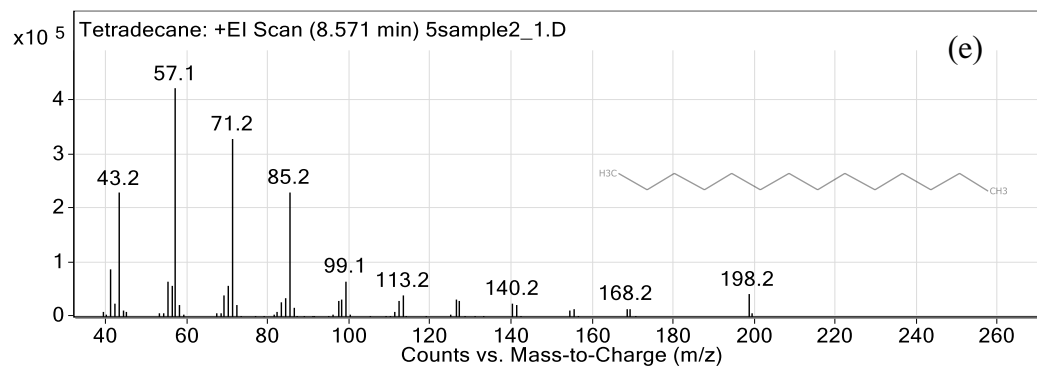
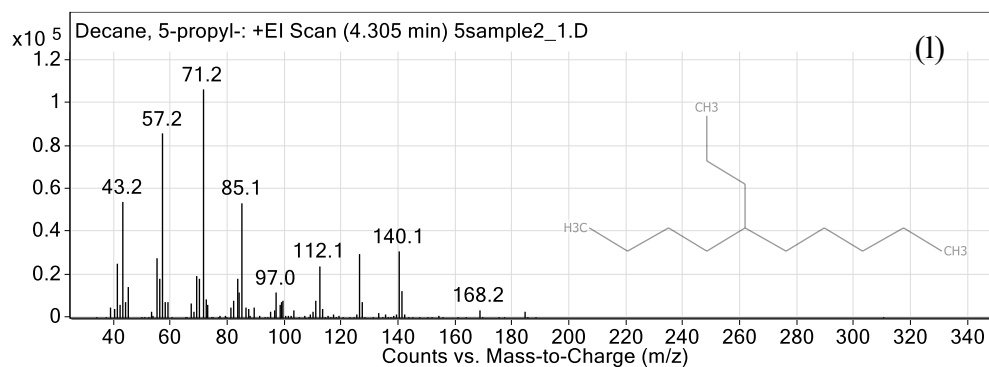
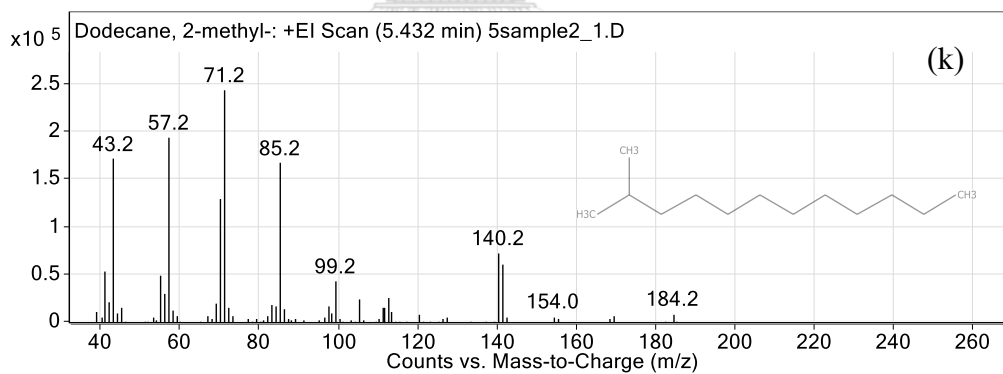
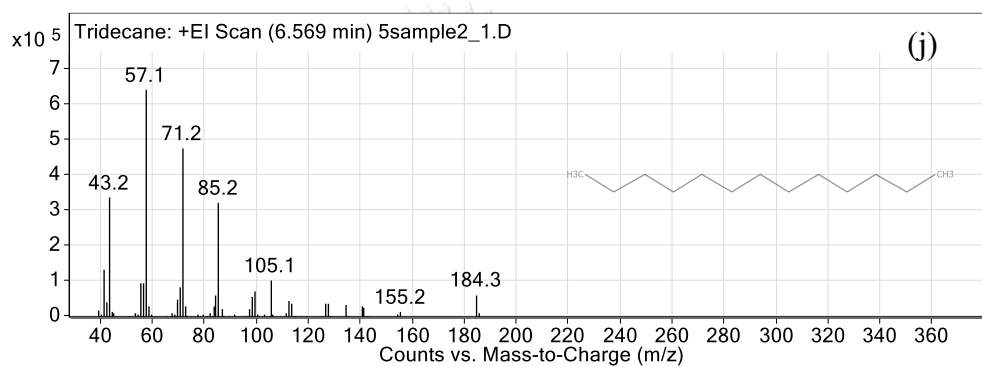
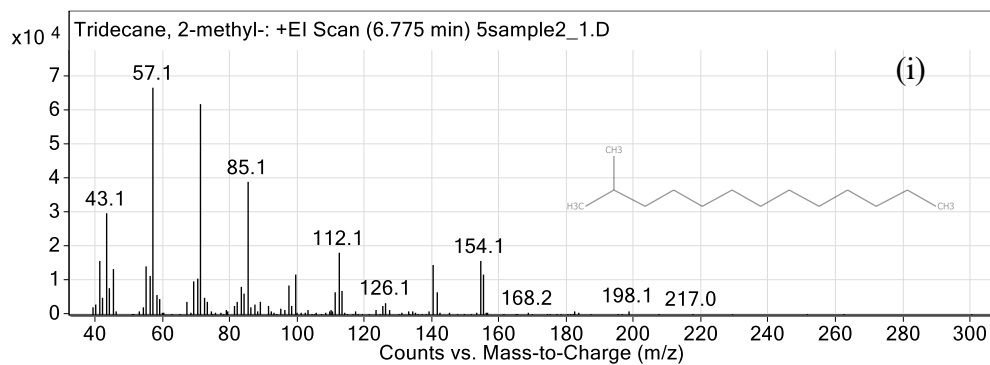


Figure A-1. MS chromatograms of liquid products (i) pre-reaction and (ii) HDO of oleic acid on Ni-Mo-S-0.2.

Condition : Temperature = 320 $^{\circ}$ C, H₂ pressure = 30 bar, catalyst weight = 0.375 wt%, oleic acid/catalyst ratio (wt/wt) = 4, and reaction time = 1 h.







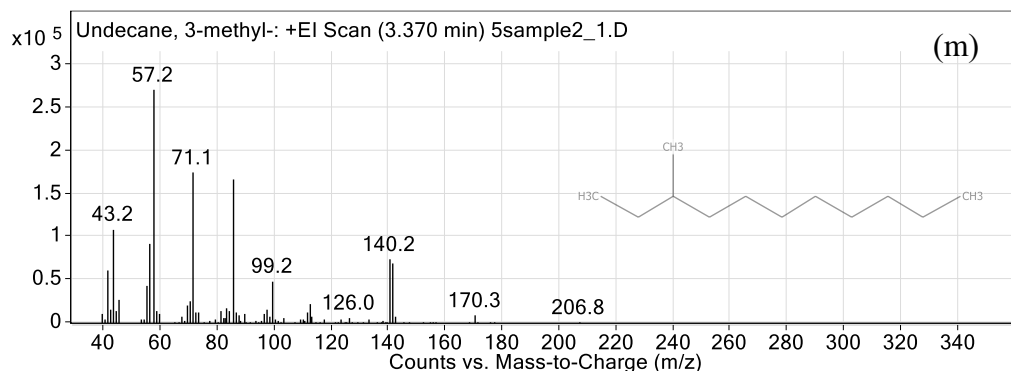


Figure A-2. MS fragmentation pattern of liquid products from HDO of oleic acid on Ni-Mo-S-0.2. (a) octadecane, (b) heptadecane, (c) hexadecane, (d) pentadecane, (e) tetradecane, (f) tridecane, 5-methyl-, (g) dodecane, 2,5-dimethyl-, (h) tridecane-, 2,5-dimethyl-, (i) tridecane, 2-methyl, (j) tridecane (k) dodecane, 2-methyl, (l) decane, 5-propyl- and (m) undecane, 3-methyl-.

Condition : Temperature = 320 °C, H₂ pressure = 30 bar, catalyst weight = 0.375 wt%, oleic acid/catalyst ratio (wt/wt) = 4, and reaction time = 1 h.

Appendix B

Calculation

a) Response Factor (R_{xi})

$$R_{xi} = \frac{M_{int}}{M_i} \times \frac{\text{Peak area of } i}{\text{Peak area of internal standard}} \quad (1)$$

where i = the standard compound

M_i = the amounts of the standard compound (g)

$M_{\text{internal standard}}$ = the internal standard (g) determined by GC-FID.

b) Amount of reactant or product after HDO reaction (W_i , wt%)

$$W_i = \frac{1}{R_{xi}} \times \frac{W_{int}}{W_{\text{sample}}} \times \frac{\text{Peak area of } i}{\text{Peak area of internal standard}} \times 100 \quad (2)$$

where i = the reactant or product

W_{int} = the weights of the internal standard (g)

W_{sample} = the weights of the liquid sample (g)

c) Conversion (wt%)

$$\text{Conversion} = \frac{C_{r \text{ in Feed}} - W_i}{C_{r \text{ in Feed}}} \times 100 \quad (3)$$

where $C_{r \text{ in feed}}$ = the concentration of reactant in feed (wt%)

W_i = the amount of reactant after reaction (wt%)

d) Selectivity (wt%)

$$\text{Selectivity} = \frac{W_i}{\sum W_i} \times 100 \quad (4)$$

where W_i = the amount of n-alkane in product (wt%)

$\sum W_i$ = the total of amount n-alkane in all products determined by GC-FID (wt%)

e) Yield (wt%)

$$\text{Yield} = \frac{W_i}{\text{Concentration of reactant}} \times 100 \quad (5)$$

where W_i = the amount of n-alkane in product determined by GC-FID (wt%).

f) n-Alkane contents (wt%)

$$\text{n-alkane contents} = \sum \text{Yield} \quad (6)$$

where $\sum \text{Yield}$ = the total yield in product (wt%).

For example:

Table B-1. Retention time, peak area and response factor of standard compound.

Compound	Weight (g)	Retention time (min)	Peak area	R _x
C ₁₄	0.1512	16.977	2454370.65	1.205921
C ₁₅	0.1508	19.251	2438354.15	1.20123
C ₁₆	0.1515	21.543	2363591.1	1.159018
C ₁₇	0.1513	23.807	2371542.1	1.164455
C ₁₈	0.1511	26.009	2206293.6	1.08475
Oleic acid	0.152	32.523	972146.05	0.475137
Methyl heptadecanoate (internal standard)	0.1619	30.381	2179296	1

From Table B-1, response factor was calculated as followings:

$$R_{x_i} = \frac{M_{\text{int}}}{M_i} \times \frac{\text{Peak area of } i}{\text{Peak area of internal standard}}$$

$$R_{x_{C_7}} = \frac{0.1619}{0.0.1513} \times \frac{2371542.1}{2179296} = 1.164455$$

$$R_{x_{C_{18}}} = \frac{0.1619}{0.1511} \times \frac{2206293.6}{2179296} = 1.08475$$

Moreover, other parameters were calculated by equation (2)-(6).

$$W_{C17} = \frac{1}{1.164455} \times \frac{3.16}{50} \times \frac{30068}{551129} \times 100 = 0.24$$

$$W_{C18} = \frac{1}{1.170259} \times \frac{3.16}{50} \times \frac{121635}{551129} \times 100 = 1.05$$

$$\text{Selectivity}_{C17} = \frac{0.24}{1.34} \times 100 = 18.1$$

$$\text{Selectivity}_{C18} = \frac{1.05}{1.34} \times 100 = 78.7$$

$$\text{Yield}_{C17} = \frac{0.24}{1.5} \times 100 = 16.9$$

$$\text{Yield}_{C18} = \frac{1.05}{1.54} \times 100 = 70.3$$

Appendix C

Data of Chromatogram

a) Effect of temperature

Condition : Temperature = 250-280 °C, H₂ pressure = 60 bar, Ni/(Ni+Mo) = 0.2, catalyst weight = 0.375 wt%, oleic acid/catalyst ratio (wt/wt) = 4, and reaction time = 6 h.

Table C-a1 250 °C			Table C-a2 280 °C		
Compounds	Area	Wi (wt%)	Compounds	Area	Wi (wt%)
C ₁₅	1900	0.01684	C ₁₅	2042	0.01599
C ₁₆	2993	0.02750	C ₁₆	3300	0.02678
C ₁₇	35175	0.32167	C ₁₇	30068	0.24291
C ₁₈	84470	0.82921	C ₁₈	121635	1.05484
Oleic acid	8400	0.18826	Oleic acid	0	0
Internal std.	529649		Internal std.	551129	

Table C-a3 300 °C			Table C-a4 320 °C		
Compounds	Area	Wi (wt%)	Compounds	Area	Wi (wt%)
C ₁₅	1500	0.01240	C ₁₅	1891	0.01551
C ₁₆	6765	0.05796	C ₁₆	6013	0.05112
C ₁₇	42414	0.36167	C ₁₇	51099	0.43240
C ₁₈	104359	0.95527	C ₁₈	97913	0.88943
Oleic acid	0	0	Oleic acid	0	0
Internal std.	545960		Internal std.	548449	

b) Effect of Pressure

Condition : Temperature = 280 °C, H₂ pressure = 60 bar, Ni/(Ni+Mo) = 0.2, catalyst weight = 0.375 wt%, oleic acid/catalyst ratio (wt/wt) = 4, and reaction time = 6 h.

Table C-b1 20 bar			Table C-b2 40 bar		
Compounds	Area	Wi (wt%)	Compounds	Area	Wi (wt%)
C ₁₅	2700	0.02305	C ₁₅	4002	0.03202
C ₁₆	7503	0.06638	C ₁₆	8200	0.06800
C ₁₇	44290	0.39001	C ₁₇	46098	0.38047
C ₁₈	77986	0.73720	C ₁₈	91899	0.81421
Oleic acid	3904	0.08425	Oleic acid	3609	0.07300
Internal std.	539649		Internal std.	551129	

Table C-b3 60 bar			Table C-b4 80 bar		
Compounds	Area	Wi (wt%)	Compounds	Area	Wi (wt%)
C ₁₅	2042	0.01599	C ₁₅	3400	0.02886
C ₁₆	3300	0.02678	C ₁₆	4480	0.03941
C ₁₇	30068	0.24291	C ₁₇	32200	0.28191
C ₁₈	121635	1.05484	C ₁₈	98100	0.92196
Oleic acid	0	0	Oleic acid	0	0
Internal std.	551129		Internal std.	550419	

c) Effect of Oleic acid/catalyst ratio

Condition : Temperature = 280 °C, H₂ pressure = 60 bar, Ni/(Ni+Mo) = 0.2, catalyst weight = 0.375 wt%, oleic acid/catalyst ratio (wt/wt) = 4, and reaction time = 6 h.

Table C-c1 1.3 (wt/wt)			Table C-c2 4 (wt/wt)		
Compounds	Area	Wi (wt%)	Compounds	Area	Wi (wt%)
C ₁₅	1309	0.01096	C ₁₅	2042	0.01599
C ₁₆	2571	0.02231	C ₁₆	3300	0.02678
C ₁₇	24022	0.20748	C ₁₇	30068	0.24291
C ₁₈	68700	0.63698	C ₁₈	121635	1.05484
Oleic acid	0	0	Oleic acid	0	0
Internal std.	531484		Internal std.	551129	

Table C-c3 8 (wt/wt)			Table C-c4 12 (wt/wt)		
Compounds	Area	Wi (wt%)	Compounds	Area	Wi (wt%)
C ₁₅	2393	0.02066	C ₁₅	2990	0.02721
C ₁₆	5824	0.05212	C ₁₆	8587.1	0.08099
C ₁₇	55004.4	0.48994	C ₁₇	100548.5	0.94390
C ₁₈	189000.2	1.80719	C ₁₈	265219	2.67269
Oleic acid	7400	0.16154	Oleic acid	10090.1	0.23214
Internal std.	556723.7		Internal std.	560710.8	

Table C-c3 1 (wt/wt)

Compounds	Area	Wi (wt%)
C ₁₅	0	0
C ₁₆	1193.1	0.00944
C ₁₇	27719.4	0.21833
C ₁₈	80354	0.67942
Oleic acid	1015.8	0.01961
Internal std.	5442636.1	

d) Effect of reaction time

Condition : Temperature = 280 °C, H₂ pressure = 60 bar, Ni/(Ni+Mo) = 0.2, catalyst weight = 0.375 wt%, oleic acid/catalyst ratio (wt/wt) = 4, and reaction time = 1-8 h.

Table C-d1 1 h

Compounds	Area	Wi (wt%)
C ₁₅	4120	0.03034
C ₁₆	5343.4	0.04079
C ₁₇	44845.8	0.34072
C ₁₈	76533.6	0.62420
Oleic acid	3939.3	0.07335
Internal std.	606010.4	

Table C-d2 3 h

Compounds	Area	Wi (wt%)
C ₁₅	2433	0.02116
C ₁₆	2371	0.02137
C ₁₇	33122	0.29709
C ₁₈	91622	0.88221
Oleic acid	1771	0.03893
Internal std.	511784	

Table C-d3 6 h

Compounds	Area	Wi (wt%)
C ₁₅	2042	0.01599
C ₁₆	3300	0.02678
C ₁₇	30068	0.24291
C ₁₈	121635	1.05484
Oleic acid	0	0
Internal std.	551129	

Table C-d4 8 h

Compounds	Area	Wi (wt%)
C ₁₅	2419	0.02099
C ₁₆	3383.1	0.03042
C ₁₇	36553.8	0.32717
C ₁₈	107430.8	1.03221
Oleic acid	0	0
Internal std.	558118	

e) **Effect of Ni/(Mo+Ni) mole ratio**

Condition : Temperature = 280 °C, H₂ pressure = 60 bar, Ni/(Mo+Ni) = 0.2, catalyst weight = 0.375 wt%, oleic acid/catalyst ratio (wt/wt) = 4, and reaction time = 6 h.

Table C-e1 0.1

Compounds	Area	Wi (wt%)
C ₁₅	2349	0.01810
C ₁₆	5061	0.04043
C ₁₇	35627.4	0.28327
C ₁₈	119997	1.02418
Oleic acid	3798	0.07401
Internal std.	601415.3	

Table C-e2 0.2

Compounds	Area	Wi (wt%)
C ₁₅	2042	0.01599
C ₁₆	3300	0.02678
C ₁₇	30068	0.24291
C ₁₈	121635	1.05484
Oleic acid	0	0
Internal std.	551129	

Table C-e3 0.3

Compounds	Area	Wi (wt%)
C ₁₅	3340	0.02255
C ₁₆	1667.3	0.01167
C ₁₇	43085.1	0.30008
C ₁₈	120572	0.90146
Oleic acid	2470	0.04216
Internal std.	618341.9	

Table C-e4 0.4

Compounds	Area	Wi (wt%)
C ₁₅	2698	0.02193
C ₁₆	1712.8	0.01443
C ₁₇	44391.9	0.37226
C ₁₈	97708.7	0.87956
Oleic acid	4516	0.09281
Internal std.	541181.1	

Table C-e3 1 NiS

Compounds	Area	Wi (wt%)
C ₁₅	0	0
C ₁₆	1477.4	0.01175
C ₁₇	12992.9	0.10282
C ₁₈	8670	0.07365
Oleic acid	9279	0.17996
Internal std.	655387.1	

f) Effect of Co/(Mo+Co) mole ratio

Condition : Temperature = 280 °C, H₂ pressure = 60 bar, Co/(Mo+Co) = 0.2, catalyst weight = 0.375 wt%, oleic acid/catalyst ratio (wt/wt) = 4, and reaction time = 6 h.

Table C-f1 0.1			Table C-f2 0.2		
Compounds	Area	Wi (wt%)	Compounds	Area	Wi (wt%)
C ₁₅	1691	0.01441	C ₁₅	1580	0.01343
C ₁₆	2047.6	0.01809	C ₁₆	7683.5	0.06769
C ₁₇	17138.2	0.15070	C ₁₇	21899.1	0.19201
C ₁₈	33567.6	0.31686	C ₁₈	66591.5	0.62678
Oleic acid	9161.8	0.19744	Oleic acid	2700	0.05802
Internal std.	548331.5		Internal std.	553347.7	

Table C-f3 0.3			Table C-f4 0.4		
Compounds	Area	Wi (wt%)	Compounds	Area	Wi (wt%)
C ₁₅	2629	0.02790	C ₁₅	2510	0.02274
C ₁₆	5499.5	0.06049	C ₁₆	2242.5	0.02105
C ₁₇	12604	0.13800	C ₁₇	11935.1	0.11154
C ₁₈	25181.2	0.29596	C ₁₈	28140.3	0.28230
Oleic acid	2898.9	0.07779	Oleic acid	5306	0.12152
Internal std.	498078.2		Internal std.	554967.9	

Table C-f3 1 CoS

Compounds	Area	Wi (wt%)
C ₁₅	1147	0.00893
C ₁₆	1299.5	0.01048
C ₁₇	9924.4	0.07970
C ₁₈	2628.2	0.02266
Oleic acid	8816.9	0.17532
Internal std.	557090.7	

g) Comparison of MoS₂

Condition : Temperature = 280 °C, H₂ pressure = 60 bar, MoS₂ = 0.2, catalyst weight = 0.375 wt%, oleic acid/catalyst ratio (wt/wt) = 4, and reaction time = 6 h.

Table C-h1 MoS₂ (Commercial)

Compounds	Area	Wi (wt%)
C ₁₅	0	0
C ₁₆	8139.4	0.07801
C ₁₇	24710	0.23573
C ₁₈	52906.9	0.54182
Oleic acid	9853.7	0.23038
Internal std.	529485.3	

Table C-h2 MoS₂ (ATTM)

Compounds	Area	Wi (wt%)
C ₁₅	871	0.00774
C ₁₆	7005.2	0.06453
C ₁₇	24388.6	0.22362
C ₁₈	61284.3	0.660322
Oleic acid	5400.4	0.12136
Internal std.	501838.6	

VITA

Miss Paphawee Sanggam was born on February 20, 1992 in Khonkaen, Thailand. She was received her Bachelor of Science degree in Chemistry, Faculty of Science, Mahidol university in 2014. She has pursued Master of Science degree in Petrochemistry and Polymer Science, Faculty of Science, Chulalongkorn University in 2015 and finished her study in 2017.

Conferences and Proceeding

"Hydrodeoxygenation of oleic acid on unsupported Co-Mo and Ni-Mo sulfide catalysts" at The 7th International Thai Institute of Chemical Engineering and Applied Chemistry Conference 2017 (ITICHE2017) and The 27th National Thai Institute of Chemical Engineering and Applied Chemistry Conference 2017 (TICHE2017), Bangkok, Thailand, 18-20 October 2017. (Poster presentation)



จุฬาลงกรณ์มหาวิทยาลัย
CHULALONGKORN UNIVERSITY